Hydrodynamics and Flow

Tetsufumi Hirano, Naomi van der Kolk, and Ante Bilandzic

1 Introduction and Disclaimer

The main purpose of the lecture was to lead students and young postdocs to the frontier of the hydrodynamic description of relativistic heavy-ion collisions (H.I.C.) in order for them to understand talks and posters presented in the Quark Matter 2008 (QM08) conference in Jaipur, India [1]. So the most recent studies were not addressed in this lecture as they would be presented during the QM08 conference itself. Also, we try to give a very pedagogical lecture here. For the readers who may want to study relativistic hydrodynamics and its application to H.I.C. as an advanced course, we strongly recommend them to consult the references.

This lecture note is divided into three parts. In the first part we give a brief introduction to relativistic hydrodynamics in the context of H.I.C. In the second part we present the formalism and some fundamental aspects of relativistic ideal and viscous hydrodynamics. In the third part, we start with some basic checks of the fundamental observables followed by discussion of collective flow, in particular *elliptic flow*, which is one of the most exciting phenomena in H.I.C. at relativistic energies. Next we discuss how to formulate the hydrodynamic model to describe dynamics of H.I.C. Finally, we conclude the third part of the lecture note by showing some results from ideal hydrodynamic calculations and by comparing them with the experimental data.

We use the natural units $c = \hbar = k_B = 1$ and the Minkowski metric $g^{\mu\nu} = \mathrm{diag}(1, -1, -1, -1)$ throughout the lecture note.

T. Hirano (✉)
Department of Physics, The University of Tokyo, Tokyo 113-0033, Japan,
hirano@phys.s.u-tokyo.ac.jp

N. van der Kolk
Nikhef, Kruislaan 409, 1098 SJ Amsterdam, The Netherlands,
kolk@nikhef.nl

A. Bilandzic
Nikhef, Kruislaan 409, 1098 SJ Amsterdam, The Netherlands,
anteb@nikhef.nl

Hirano, T. et al.: *Hydrodynamics and Flow*. Lect. Notes Phys. **785**, 139–178 (2010)
DOI 10.1007/978-3-642-02286-9_4

2 Introduction to Hydrodynamics in Relativistic Heavy-Ion Collisions

The excitement raised by the announcement of the discovery of the "perfect" liquid at Relativistic Heavy Ion Collider (RHIC) in Brookhaven National Laboratory (BNL) [2] is based on an agreement between predictions from *ideal* hydrodynamic models with the experimental data. While this agreement was certainly a large boost for various groups around the world doing research in hydrodynamics (and even in string theory!), there are also other reasons why the usage of hydrodynamics is strongly needed in H.I.C. Needless to say, the main goals of the physics of H.I.C. are to discover the deconfined nuclear matter under equilibrium, namely the Quark–gluon plasma (QGP), and to understand its properties such as equation of state (EoS), temperature and order of phase transition, transport coefficients, and so on. However, the system produced in H.I.C. dynamically evolves within time duration of the order of 10–100 fm/c. Hence one has to describe space–time evolution of thermodynamic variables to fill a large gap between the static aspects of QGP properties and dynamical aspects of H.I.C. It is the hydrodynamics that plays an important role in connecting them. Various stages of H.I.C. are depicted in Fig. 1. Two energetic nuclei are coming along light cone and collide with each other to create a multi-parton system. Through secondary collisions the system may reach thermal equilibrium and the QGP can be formed. This is a transient state: After further expansion and cooling the system hadronizes again. Eventually, expansion leads to a free-streaming stage through freezeout and particle spectra at this moment are seen by the detector. Hydrodynamics is applied to matter under local equilibrium in the intermediate stage. Of course, it is nontrivial a priori whether one can always apply hydrodynamics to the dynamics of H.I.C. Nevertheless it is not a bad idea to

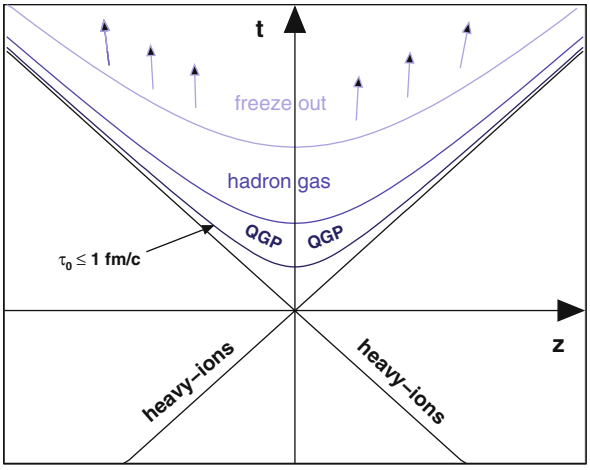

Fig. 1 A schematic view of dynamics of a heavy-ion collision along the collision axis

dare to apply it since we are eager to understand the matter under equilibrium in terms of H.I.C.

There is also another good reason to apply hydrodynamics to H.I.C. A lot of experimental data have been published so far at various collision energies. Ideally, one may want to describe these data from the first principle, i.e., quantum chromodynamics (QCD). The QCD Lagrangian density reads

$$\mathcal{L} = \bar{\psi}_i \left(i\gamma_\mu D^\mu_{ij} - m\delta_{ij} \right) \psi_j - \frac{1}{4} F_{\mu\nu\alpha} F^{\mu\nu\alpha}, \tag{1}$$

where ψ_i is a quark field, $i(= 1\text{–}3)$ is a color index for quarks, D^μ is a covariant derivative, m is a quark mass, $F^{\mu\nu}_\alpha$ is a field strength of gluons, and $\alpha(= 1, \ldots, 8)$ is a color index for gluons. However, in spite of its simple-looking Lagrangian, it is very difficult to make any predictions directly from QCD in H.I.C. due to its complexity which mainly arises from nonlinearity of interactions of gluons, strong coupling, dynamical many body system, and color confinement. One promising strategy to connect the first principle with phenomena is to introduce hydrodynamics as a phenomenological theory. We call this strategy a bottom-up approach to H.I.C. An input to this phenomenological theory comprises the equation of state,

$$P = P(e, n), \tag{2}$$

which expresses the pressure P as a function of energy density e and baryon density n. This can be obtained by exploiting lattice numerical simulations of QCD.[1] In the case of viscous hydrodynamics we need additionally the transport coefficients such as shear viscosity η, bulk viscosity ζ, heat conductivity λ.[2]

Once hydrodynamics turns out to work quite well in the description of dynamics, one can utilize its outputs such as local temperature or energy density for other observables. In the current formalism of jet quenching, one needs an information of parton density or energy density along a trajectory of an energetic parton [3, 4]. If one assumes J/ψ melts away above some temperature [5], one needs local temperature at the position of J/ψ. In the case of electromagnetic probes [6, 7], one convolutes emission rate (the number of produced particles per unit space–time volume at temperature T) of thermal photons and dileptons over the space–time volume under equilibrium. Hydrodynamics provides us with the information of the bulk matter. Therefore we can say that, in the context of H.I.C., hydrodynamics is the heart of the dynamical modeling: It not only describes expansion and collective flow of matter but also provides important information in the intermediate stage for other phenomena.

---

[1] From lattice calculations, pressure as a function of temperature rather than energy density is obtained. Note also that, due to sign problem, thermodynamic variables are available only near the region of vanishing chemical potential.

[2] In principle, the information about these quantities can be obtained also from the lattice QCD simulations although it is much harder than the EoS.

3 Formalism of the Relativistic Ideal/Viscous Hydrodynamics

The second part of the lecture note is more formal with many equations, but we try as much as possible to provide the intuitive picture behind the equations. The following references might be very helpful to complement this section [8–24].

3.1 The Basic Equations

The basic hydrodynamical equations are energy–momentum conservation

$$\partial_\mu T^{\mu\nu} = 0\,, \tag{3}$$

where $T^{\mu\nu}$ is the energy–momentum tensor and the current conservation

$$\partial_\mu N_i^\mu = 0\,, \tag{4}$$

where N_i^μ is the ith conserved current. In H.I.C., there are some conserved charges such as baryon number, strangeness, electric charges, and so on. We mainly assume the net baryon current N_B^μ as an example of N_i^μ in the following. In the first step we decompose the energy–momentum tensor and the conserved current as follows:

$$T^{\mu\nu} = eu^\mu u^\nu - P\Delta^{\mu\nu} + W^\mu u^\nu + W^\nu u^\mu + \pi^{\mu\nu}\,, \tag{5}$$

$$N_i^\mu = n_i u^\mu + V_i^\mu\,. \tag{6}$$

All the terms in the above expansion will be discussed one by one later. Now we indicate that u^μ is the time-like, normalized four-vector

$$u_\mu u^\mu = 1\,, \tag{7}$$

while the tensor $\Delta^{\mu\nu}$ is defined in the following way:

$$\Delta^{\mu\nu} = g^{\mu\nu} - u^\mu u^\nu\,, \tag{8}$$

where $g^{\mu\nu}$ is the Minkowski metric. We refer to u^μ and $\Delta^{\mu\nu}$ as the "projection" vector and tensor operators, respectively. In particular, u^μ is the local flow four-velocity, but a more precise meaning will be given later. u^μ is perpendicular to $\Delta^{\mu\nu}$, as can easily be seen from the definition of $\Delta^{\mu\nu}$ given in Eq. (8) and from the fact that u^μ is normalized,

$$u_\mu \Delta^{\mu\nu} = u_\mu (g^{\mu\nu} - u^\mu u^\nu) = u^\nu - 1 \cdot u^\nu = 0\,. \tag{9}$$

Next we define the local rest frame (LRF) as the frame in which u^μ has only the time-like component nonvanishing and in which $\Delta^{\mu\nu}$ has only the space-like components nonvanishing, i.e.,

$$u^\mu_{\rm LRF} = (1, 0, 0, 0)\,, \tag{10}$$
$$\Delta^{\mu\nu}_{\rm LRF} = {\rm diag}(0, -1, -1, -1)\,. \tag{11}$$

As is easily understood from the above equations, one can say that $u^\mu(\Delta^{\mu\nu})$ picks up the time-(space-)like component(s) when acting on some Lorentz vector/tensor.

We now discuss the physical meaning of each term in the expansion of the energy–momentum tensor (5) and the conserved current (6).

3.1.1 Decomposition of $T^{\mu\nu}$

The new quantities which appear on the RHS in the decomposition (5) are defined in the following way:

$$e = u_\mu T^{\mu\nu} u_\nu \quad \text{(energy density)}\,, \tag{12}$$
$$P = P_s + \Pi = -\frac{1}{3}\Delta_{\mu\nu} T^{\mu\nu} \quad \text{(hydrostatic + bulk pressure)}\,, \tag{13}$$
$$W^\mu = \Delta^\mu{}_\alpha T^{\alpha\beta} u_\beta \quad \text{(energy (or heat) current)}\,, \tag{14}$$
$$\pi^{\mu\nu} = \langle T^{\mu\nu} \rangle \quad \text{(shear stress tensor)}\,. \tag{15}$$

Each term corresponds to projection of the energy–momentum tensor by one or two projection operator(s), u^μ and $\Delta^{\mu\nu}$. The first two equalities imply that the energy density e can be obtained from the time-like components of the energy–momentum tensor, while the pressure P is obtained from the space-like components. Contracting the energy–momentum tensor simultaneously with u^μ and $\Delta^{\mu\nu}$ gives the energy (heat) current W^μ. Finally, the angular brackets in the definition of the shear stress tensor $\pi^{\mu\nu}$ stand for the following operation:

$$\langle A^{\mu\nu} \rangle = \left[\frac{1}{2}(\Delta^\mu{}_\alpha \Delta^\nu{}_\beta + \Delta^\mu{}_\beta \Delta^\nu{}_\alpha) - \frac{1}{3}\Delta^{\mu\nu}\Delta_{\alpha\beta} \right] A^{\alpha\beta}\,. \tag{16}$$

This means that $\langle A^{\mu\nu} \rangle$ is a symmetric and traceless tensor which is transverse to u^μ and u^ν. More concretely, one can first decompose the energy–momentum tensor by two projection tensors symmetrically

$$\tilde{\pi}^{\mu\nu} = \frac{1}{2}(\Delta^\mu{}_\alpha T^{\alpha\beta} \Delta_\beta{}^\nu + \Delta^\nu{}_\alpha T^{\alpha\beta} \Delta_\beta{}^\mu) \tag{17}$$

and then decompose it once more into the shear stress tensor (traceless) and the pressure (non-traceless)

$$\tilde{\pi}^{\mu\nu} = \pi^{\mu\nu} - P\Delta^{\mu\nu}. \tag{18}$$

3.1.2 Decomposition of N^μ

In the decomposition (6) we have introduced the following quantities:

$$n_i = u_\mu N_i^\mu \quad \text{(charge density)}\,, \tag{19}$$
$$V_i^\mu = \Delta^\mu_{\ \nu} N_i^\nu \quad \text{(charge current)}\,. \tag{20}$$

The physical meaning of n_i and V_i^μ is self-evident from the properties of projection operators.

QUESTION 1: *Count the number of unknowns in the above decompositions and confirm that it is* $10(T^{\mu\nu}) + 4k(N_i^\mu)$. *Here* k *is the number of independent currents.*[3]

The various terms appearing in the decompositions (5) and (6) can be grouped into two distinctive parts, which we call ideal and dissipative. In particular, for the energy–momentum tensor we have

$$T^{\mu\nu} = T_0^{\mu\nu} + \delta T^{\mu\nu}\,, \tag{21}$$
$$T_0^{\mu\nu} = eu^\mu u^\nu - P_s\Delta^{\mu\nu}\,, \tag{22}$$
$$\delta T^{\mu\nu} = -\Pi\Delta^{\mu\nu} + W^\mu u^\nu + W^\nu u^\mu + \pi^{\mu\nu}\,, \tag{23}$$

while for one charge current we have,

$$N^\mu = N_0^\mu + \delta N^\mu\,, \tag{24}$$
$$N_0^\mu = nu^\mu\,, \tag{25}$$
$$\delta N^\mu = V^\mu\,. \tag{26}$$

In the above relations $T_0^{\mu\nu}(N_0^\mu)$ denote the ideal part, while the $\delta T^{\mu\nu}(\delta N^\mu)$ denote the dissipative part of the $T^{\mu\nu}(N^\mu)$.

3.2 The Meaning of u^μ

As we have already mentioned in Sect. 3.1, u^μ is the four-velocity of "flow." Now we would like to clarify what kind of flow we have in mind in this description. In literature two definitions of flow can be found

[3] If you consider u^μ as independent variables, you need additional constraint for them since these are redundant ones. If you also consider P_s as an independent variable, you need the equation of state $P_s = P_s(e, n)$.

1. flow of energy (Landau) [10]:

$$u_L^\mu = \frac{T^\mu{}_\nu\, u_L^\nu}{\sqrt{u_L^\alpha T_\alpha{}^\beta T_{\beta\gamma} u_L^\gamma}} = \frac{1}{e} T^\mu{}_\nu\, u_L^\nu\,, \tag{27}$$

2. flow of conserved charge (Eckart) [8]:

$$u_E^\mu = \frac{N^\mu}{\sqrt{N_\nu N^\nu}} \tag{28}$$

(see Fig. 2).[4] In the first definition, u_L^μ also appears on the RHS of Eq. (27). So it should be understood as an equation with respect to u_L^μ. One may solve an eigenvalue problem for a given energy–momentum tensor $T^\mu{}_\nu \cdot u_L^\mu$ is a normalized time-like eigenvector and the corresponding positive eigenvalue is energy density e. If the dissipative currents are small enough, one can show the following relation between these two definitions of flow:

$$u_L^\mu \approx u_E^\mu + \frac{W^\mu}{e + P_s}, \quad u_E^\mu \approx u_L^\mu + \frac{V^\mu}{n}. \tag{29}$$

Equation (29) can be shown by assuming that both two definitions of flow can be connected by infinitesimal proper Lorentz transformation

$$u_E^\mu = a^\mu{}_\nu u_L^\nu \tag{30}$$

$$\approx (\delta^\mu{}_\nu + \epsilon^\mu{}_\nu) u_L^\nu, \tag{31}$$

where $\epsilon^\mu{}_\nu$ is infinitesimal anti-symmetric tensor, and by neglecting the higher orders of dissipative currents. Obviously, $W^\mu = 0$ ($V^\mu = 0$) in the Landau (Eckart) frame. In the case of vanishing dissipative currents, both definitions represent a common

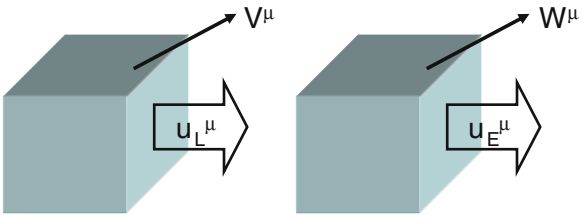

Fig. 2 A sketch of Landau and Eckart definitions of flow. Two boxes are fluid elements. There is a "leak" current W^μ or V^μ according to the definition of flow

[4] Other definitions can be made. The situation here is quite similar to the gauge fixing condition in gauge theories to eliminate the redundant variables. An essential point is to choose some "gauge" for later convenience.

flow. In other words, flow is uniquely determined in the case of ideal hydrodynamics. We should emphasize that Landau definition is more relevant in the context of H.I.C. at ultrarelativistic energies since we expect that a small baryon number is deposited near the midrapidity region.

3.3 Entropy

We start this subsection by briefly discussing the entropy conservation in "ideal hydrodynamics." By "ideal hydrodynamics" we mean the case when entropy is not produced during the evolution.[5] Neglecting the dissipative parts, the energy–momentum conservation (3) and the current conservation (4) reduce to

$$\partial_\mu T_0^{\mu\nu} = 0\,, \tag{32}$$

$$\partial_\mu N_0^{\mu} = 0\,, \tag{33}$$

where $T_0^{\mu\nu}$ and N_0^{μ} are the ideal parts introduced in Eqs. (22) and (25). Equations (32) and (33) are the basic equations of "ideal hydrodynamics."

By contracting Eq. (32) with u_ν it follows

$$\begin{aligned} 0 &= u_\nu \partial_\mu T_0^{\mu\nu} \\ &= \dots \\ &= T(u^\mu \partial_\mu s + s\partial_\mu u^\mu) + \mu(u^\mu \partial_\mu n + n\partial_\mu u^\mu)\,. \end{aligned} \tag{34}$$

We have introduced here the temperature T, entropy density s, and chemical potential μ through the first law of thermodynamics $de = Tds + \mu dn$. Here it is assumed that thermalization is maintained locally. The second term on the RHS in Eq. (34) vanishes due to Eq. (33). If we now introduce the entropy current as

$$S^\mu = su^\mu\,, \tag{35}$$

it follows from Eq. (34) that

$$\partial_\mu S^\mu = \partial_\mu(su^\mu) = u^\mu \partial_\mu s + s\partial_\mu u^\mu = 0\,. \tag{36}$$

Hence the entropy is conserved in ideal hydrodynamics.

QUESTION 2: *Go through all steps in the above derivations.*

Now we go back to viscous hydrodynamics. Hereafter we consider only the Landau frame and omit the subscript L. For simplicity, we further assume that there is no charge in the system although in the realistic case a small amount of charge might

[5] Note that, if discontinuities exist in the solution, entropy is produced even in ideal hydrodynamics.

exist in the system. What we are constructing here is the so-called first-order theory of viscous hydrodynamics. The main assumption is that the nonequilibrium entropy current vector S^μ has linear dissipative term(s) constructed from V^μ, Π, and $\pi^{\mu\nu}$ and can be written as

$$S^\mu = su^\mu + \alpha V^\mu \,. \tag{37}$$

The first term on the RHS is the ideal part and the second term is the correction due to the dissipative part. It is impossible to construct a term which would form a Lorentz vector from $\pi^{\mu\nu}$ on the RHS in the above equation because $\pi^{\mu\nu}$ is perpendicular to u^μ by definition.[6] Since we have also assumed that there is no charge in the system, i.e., $N^\mu = 0$, it follows that αV^μ vanishes.

We now calculate the product of the temperature T and the divergence of the entropy current (37). It follows

$$\begin{aligned} T\partial_\mu S^\mu &= T(u^\mu \partial_\mu s + s\partial_\mu u^\mu) \\ &= u_\nu \partial_\mu T_0^{\mu\nu} \\ &= -u_\nu \partial_\mu \delta T^{\mu\nu} \\ &= \dots \\ &= \pi_{\mu\nu} \langle \nabla^\mu u^\nu \rangle - \Pi \partial_\mu u^\mu \,, \end{aligned} \tag{38}$$

where $\nabla^\mu = \Delta^{\mu\nu}\partial_\nu$. In transferring from the second to third line in the above calculation we have used the energy–momentum conservation, $\partial_\mu T^{\mu\nu} = 0$. It is very important to note that due to the assumption that there is no charge in the system we could neglect the dissipative part of entropy current (37), but the dissipative part of energy–momentum tensor (23) does not vanish. The nonvanishing dissipative part of energy–momentum tensor gives a contribution which yields a difference between the equations characterizing the first-order theory of viscous hydrodynamics and the equations of ideal hydrodynamics derived before.

QUESTION 3: *Check the above calculation.*

In order to solve the hydrodynamic equations we must first define the dissipative current. We introduce the following two phenomenological definitions, so-called *constitutive equations*, for the shear stress tensor $\pi^{\mu\nu}$ and the bulk pressure Π:

$$\pi^{\mu\nu} = 2\eta \langle \nabla^\mu u^\nu \rangle \,, \tag{39}$$

$$\Pi = -\zeta \partial_\mu u^\mu = -\zeta \nabla_\mu u^\mu \,. \tag{40}$$

---

[6] Also remember $W^\mu = 0$ in the Landau definition. One may think that Πu^μ is a possible candidate in the entropy current S^μ. However, the second law of thermodynamics is not ensured in this case. See also discussion in [21].

In Table 1 we outline the new variables and terminology used in the above equations. Notice that, within our approximation $N^\mu = 0$, there is no vector component of thermodynamic force.

Table 1 New variables and terminology

Thermodynamic force	Transport coefficient	Current
$X^{\mu\nu} = \langle \nabla^\mu u^\nu \rangle$	η	$\pi_{\mu\nu}$
tensor	shear viscosity	
$X = -\partial_\mu u^\mu$	ζ	Π
scalar	bulk viscosity	

After inserting the definitions (39) and (40) in the last line of (38), we arrive at, for positive transport coefficients,

$$\begin{aligned} T\,\partial_\mu S^\mu &= \frac{\pi_{\mu\nu}\pi^{\mu\nu}}{2\eta} + \frac{\Pi^2}{\zeta} \\ &= 2\eta\,\langle \nabla^\mu u^\nu \rangle^2 + \zeta\left(-\partial_\mu u^\mu\right)^2 \geq 0\,. \end{aligned} \tag{41}$$

This ensures the second law of thermodynamics

$$\partial_\mu S^\mu \geq 0\,. \tag{42}$$

In the case of viscous hydrodynamics, entropy is not decreasing.

3.4 The Equations of Motion

In order to derive the equations of motion, we use again energy–momentum conservation (3). After contracting Eq. (3) with u_ν we have

$$u_\nu \partial_\mu T^{\mu\nu} = 0\,, \tag{43}$$

from which one can obtain the first equation of motion,

$$\dot{e} = -(e + P_s + \Pi)\theta + \pi_{\mu\nu}\,\langle \nabla^\mu u^\nu \rangle\ . \tag{44}$$

On the other hand, after contracting Eq. (3) with $\Delta_{\mu\alpha}$ it follows

$$\Delta_{\mu\alpha}\partial_\beta T^{\alpha\beta} = 0\,, \tag{45}$$

from which one can obtain the second equation of motion,

$$(e + P_s + \Pi)\dot{u}^\mu = \nabla^\mu(P_s + \Pi) - \Delta^{\mu\alpha}\nabla^\beta \pi_{\alpha\beta} + \pi^{\mu\alpha}\dot{u}_\alpha\,. \tag{46}$$

This is exactly the relativistic extension of the Navier–Stokes equation. In writing the above equations we have introduced

$$\theta = \partial_\mu u^\mu \qquad \text{expansion scalar (divergence of flow)}, \tag{47}$$

$$\text{“dot”} = D = u_\mu \partial^\mu \qquad \text{substantial time derivative}\,. \tag{48}$$

QUESTION 4: *Starting from the energy–momentum conservation* (3) *derive Eqs.* (44) *and* (46).

To get some intuitive interpretation of the first equation of motion, we insert expressions (39) and (40) for the shear stress tensor and bulk pressure into Eq. (44):

$$\begin{aligned}\dot{e} &= -e\theta - P_s\theta + \frac{\Pi^2}{\zeta} + \frac{\pi_{\mu\nu}\pi^{\mu\nu}}{2\eta} \\ &= -e\theta - P_s\theta + \zeta(-\theta)^2 + 2\eta\,\langle\nabla^\mu u^\nu\rangle^2\,.\end{aligned} \tag{49}$$

The above equation determines the time evolution of energy density e in the comoving system. The first term on the RHS describes dilution/compression of energy density due to the change of volume because θ can be expressed in terms of volume of a fluid element V as

$$\theta \approx \frac{\dot{V}}{V}\,. \tag{50}$$

In ideal hydrodynamics, this relation holds exactly. If the system expands ($\theta > 0$), the energy density is diluted. So the effect of expansion appears as negative source term $-e\theta$ in Eq. (49). If we move along with a fluid element, the internal energy in the fluid element is not conserved due to the work done by pressure, which is described by the second term on the RHS in (49). Finally, the last two positive definite terms in (49) represent the production of entropy which heats up the system.

Now we comment on the second equation of motion (46). But before doing that, we recall the nonrelativistic Navier–Stokes equation,

$$D\boldsymbol{v} = -\frac{1}{\rho}\boldsymbol{\nabla} P_s + \frac{\eta}{\rho}\boldsymbol{\nabla}^2\boldsymbol{v}\,. \tag{51}$$

Here ρ is the mass density, η is shear viscosity, and $D = \frac{\partial}{\partial t} + \boldsymbol{v}\cdot\boldsymbol{\nabla}$ is the nonrelativistic version of substantial time derivative. The above version of the nonrelativistic Navier–Stokes equation applies to the case of incompressible fluids such that $\boldsymbol{\nabla}\cdot\boldsymbol{v} = 0$ is valid. On the LHS we have the time derivative of velocity, which is nothing but acceleration. The first term on the RHS is the source of the flow and it is solely due to the pressure gradient $\boldsymbol{\nabla} P_s$, while the second term represents the diffusion of the flow. The final flow velocity comes from the interplay between these two terms: The first term generates the flow while the second term dilutes it. The ratio η/ρ is called kinetic viscosity and plays a role of diffusion constant

in the Navier–Stokes equation (51). The diffusion term in Eq. (51) requires more detailed treatment. For an illustrative purpose, consider first the heat equation in (N+1)-dimensional space–time

$$\frac{\partial T(t,\{x_i\})}{\partial t} = \kappa \sum_i^N \frac{\partial^2}{\partial x_i^2} T(t,\{x_i\}), \tag{52}$$

where T is temperature and constant κ is heat conductivity in some unit. One can discretize the heat equation (52) in $(2+1)$-dimensional space–time as follows:

$$\begin{aligned} T_{i,j}^{n+1} &= T_{i,j}^n + \frac{4\kappa\Delta t}{(\Delta x)^2}\left[\frac{T_{i-1,j}^n + T_{i,j-1}^n + T_{i+1,j}^n + T_{i,j+1}^n}{4} - T_{i,j}^n\right] \\ &= T_{i,j}^n + \frac{4\kappa\Delta t}{(\Delta x)^2}\left(\bar{T}_{i,j}^n - T_{i,j}^n\right), \end{aligned} \tag{53}$$

where i and j are indices of the site and n is the time step. The first term in the brackets in Eq. (53), $\bar{T}_{i,j}$, indicates an average of temperature around the cell under consideration. If temperature at (i, j) is smaller (larger) than the averaged one $\bar{T}_{i,j} > T_{i,j}$ ($\bar{T}_{i,j} < T_{i,j}$), the second term in Eq. (53) becomes positive (negative) and, consequently, temperature increases (decreases) in the next time step. Repeating this procedure, temperature becomes flat even if starting from a bumpy initial condition. Thus, generally speaking, the second derivative with respect to coordinates describes averaging/smoothening/diffusion of given distributions and a coefficient in front of it describes how quick the distribution diffuses. Now going back to the Navier–Stokes equation (51), it is obvious from the above discussion that the second term describes diffusion of flow and that kinetic viscosity η/ρ plays a role of a diffusion constant. The relativistic version of the Navier–Stokes equation (46) has a similar form to Eq. (51) if one plugs in constitutive equations (39) and (40) and assumes the fluid is incompressible, $\theta = 0$.

3.4.1 Bjorken's Equation in the First-Order Theory

Now we rewrite again the first equation of motion by making use of Bjorken's ansatz [16]

$$u_{\mathrm{Bj}}^\mu = \frac{\tilde{x}^\mu}{\tau} = \frac{t}{\tau}\left(1, 0, 0, \frac{z}{t}\right), \tag{54}$$

where $\tau = \sqrt{t^2 - z^2}$ is the proper time. This is a boost-invariant Bjorken's solution which is also called one-dimensional Hubble flow since velocity in the z-direction, v_z, is proportional to z, which is an analogy to three-dimensional Hubble flow of the universe. After inserting this solution into the constitutive equations (39) and (40)

$$\pi^{\mu\nu} = \frac{2\eta}{\tau}\left(\tilde{\Delta}^{\mu\nu} - \frac{1}{3}\Delta^{\mu\nu}\right), \tag{55}$$

$$\tilde{\Delta}^{\mu\nu} = \tilde{g}^{\mu\nu} - u^{\mu}_{\mathrm{Bj}} u^{\nu}_{\mathrm{Bj}}, \quad \tilde{g}^{\mu\nu} = \mathrm{diag}(1, 0, 0, -1), \tag{56}$$

$$\Pi = -\frac{\zeta}{\tau}, \tag{57}$$

we arrive at the following equation of motion:

$$\frac{de}{d\tau} = -\frac{e + P_s}{\tau}\left(1 - \frac{4}{3\tau T}\frac{\eta}{s} - \frac{1}{\tau T}\frac{\zeta}{s}\right). \tag{58}$$

This equation determines the time evolution of energy density in the first-order theory in one-dimensional expansion.

QUESTION 5: *Derive Eq.* (58).

On the RHS of (58) we have three terms in the bracket. If we neglect the last two terms this equation reduces to the famous Bjorken equation [16] which states that in ideal hydrodynamics the energy density evolution is determined by the sum of energy density e and the hydrostatic pressure P_s, divided by the proper time τ. The last two terms on the RHS in (58) represent the viscous correction to ideal hydrodynamics. The first one is the viscous correction originating from the shear viscosity in compressible fluids while the second one comes from the bulk viscosity. We remark that both terms are proportional to $1/\tau$ which is due to the fact that the expansion scalar θ in the Bjorken scaling solution can be written as

$$\theta = \frac{1}{\tau}. \tag{59}$$

Two transport coefficients in the viscous correction, η/s and ζ/s, turn out to be very important. They are the dimensionless quantities in natural units and reflect the intrinsic properties of the fluids.[7]

Recently progress has been made in obtaining the values of the transport coefficients from microscopic theories. Here we summarize the most important results and conclusions as follows:

- $\eta/s = 1/4\pi$ and $\zeta/s = 0$ are obtained from $\mathcal{N} = 4$ SUSY Yang–Mills theory [25]. The latter one is automatically obtained from the conformal nature of the theory;
- $\eta/s = \mathcal{O}(0.1 - 1)$ for gluonic matter is obtained from the lattice calculations of pure SU(3) gauge theory [26];

[7] We stress that in the context of H.I.C. the statement which is often used, "viscosity is small," is not precise. From the equations we have derived, we see that the correct statement should be "viscous coefficients are small in comparison with entropy density."

- bulk viscosity has a prominent peak around T_c resulting from trace anomaly of QCD [27, 28] (see also a phenomenological approach in [29]).

3.5 The Second-Order Theory and Its Application to Bjorken's Equation

There is an important issue in the first-order theory which is the violation of causality. We can trace back the origin of the violation of causality to our phenomenological definitions (39) and (40) for the shear stress tensor and the bulk pressure, respectively, and to the fact that the Navier–Stokes equation is a parabolic equation, namely the time derivative is of first order while the space derivative is of second order. The same arguments hold also for the violation of causality in relativistic hydrodynamics: It is known that, under linear perturbations on the moving background equilibrium state, the solutions are unstable and acausal [30] (for a more detailed discussion, see also a recent study in [31]). For an illustrative purpose, we continue this discussion by analyzing the heat equation as an example of the parabolic equation in three-dimensional space,[8]

$$\frac{\partial T}{\partial t} = \kappa \sum_i^3 \frac{\partial^2}{\partial x_i^2} T \,. \tag{60}$$

The heat equation can be easily derived by combining the balance equation,

$$\frac{\partial T}{\partial t} = -\frac{\partial q^i}{\partial x^i} \,, \tag{61}$$

together with the constitutive equation,

$$q^i = -\kappa \frac{\partial T}{\partial x_i} \qquad \text{Fourier's law.} \tag{62}$$

In the above equations T is the temperature, q^i is the heat current, and κ is the heat conductivity. The above constitutive equation is purely phenomenological. Although here we are considering the nonrelativistic equations, the general arguments and conclusions we write down are valid in the relativistic case as well. The heat equation (60) violates causality. It can be easily confirmed that Green's function of the heat equation (60), sometimes called heat kernel, is Gaussian

$$G(x^i, t; x_0^i, t_0) = \frac{1}{[4\pi\kappa(t-t_0)]^{\frac{3}{2}}} \exp\left[-\frac{(x^i - x_0^i)^2}{4\kappa(t-t_0)}\right] \tag{63}$$

[8] Again, we choose some units to simplify the following equations:

and the "long tail" of this Gauss function causes the violation of causality in the heat equation. This issue was heuristically resolved by Cattaneo in 1948 [9] after an additional term on the LHS of the constitutive equation (62) was introduced "by hand,"

$$\tau_r \frac{\partial q^i}{\partial t} + q^i = -\kappa \frac{\partial T}{\partial x_i} \,. \tag{64}$$

In the modified constitutive equation we have a new constant τ_r which is often called the "relaxation time." Correspondingly, the heat equation (60) is also modified,

$$\tau_r \frac{\partial^2 T}{\partial t^2} + \frac{\partial T}{\partial t} = \kappa \frac{\partial^2 T}{\partial x_i^2} \,, \qquad c_s = \sqrt{\kappa/\tau_r} \,. \tag{65}$$

In the literature the above equation is known as a telegraph equation. While the original heat equation can be classified as a parabolic equation, the telegraph equation belongs to the family of hyperbolic equations. Causality is not violated in Eq. (65) simply because we can now, by choosing the relaxation time τ_r to be large, reduce the signal velocity c_s to values smaller than the speed of light c.

In relativistic hydrodynamics the relaxation terms introduced above can be obtained by modifying the entropy current in the following way:

$$S^\mu = s u^\mu + \mathcal{O}(\delta T^{\mu\nu}) + \mathcal{O}\left((\delta T^{\mu\nu})^2\right) \,. \tag{66}$$

By including the quadratic dissipative terms we are starting to work within the framework of second-order theory. The nonequilibrium entropy current vector S^μ in the second-order theory has linear + quadratic dissipative term(s) constructed from $(V^\mu, \Pi, \pi^{\mu\nu})$. Again, we demand the second law of thermodynamics, $\partial_\mu S^\mu > 0$. Thus, quadratic dissipative terms modify the constitutive equations which now read as

$$\tau_\pi \Delta^{\mu\alpha} \Delta^{\nu\beta} \dot{\pi}_{\alpha\beta} + \pi^{\mu\nu} = 2\eta \langle \nabla^\mu u^\nu \rangle + \cdots \,, \tag{67}$$

$$\tau_\Pi \dot{\Pi} + \Pi = -\zeta \partial_\mu u^\mu + \cdots \,. \tag{68}$$

When compared to the constitutive equations of the first-order theory, (39) and (40), we see that in the second-order theory in each constitutive equation a relaxation term appears. Relaxation terms include τ_π and τ_Π, which are the relaxation times. It is important to note that in the second-order theory the constitutive equations are no longer algebraic equations. As a consequence, dissipative currents become dynamical quantities like thermodynamic variables. The constitutive equations with relaxation terms have been employed in recent viscous fluid simulations [32–45].[9]

[9] Some of the references here do not employ the same equations as mentioned here. There are still some hot debates how to formulate the correct *relativistic* equation of viscous fluids or which terms in the constitutive equations of the second-order theory should be kept in the simulations.

Finally, we outline Bjorken's equation in the second-order theory,

$$\frac{de}{d\tau} = -\frac{e+P_s}{\tau}\left(1 - \frac{\pi}{sT} + \frac{\Pi}{sT}\right), \tag{69}$$

$$\tau_\pi \frac{d\pi}{d\tau} + \pi = \frac{4\eta}{3\tau} - \frac{\pi\tau_\pi}{2\tau} - \frac{\pi\eta T}{2}\frac{d}{d\tau}\frac{\tau_\pi}{\eta T}, \tag{70}$$

$$\tau_\Pi \frac{d\Pi}{d\tau} + \Pi = -\frac{\zeta}{\tau} - \frac{\Pi\tau_\Pi}{\tau} - \frac{\Pi\zeta T}{2}\frac{d}{d\tau}\frac{\tau_\Pi}{\zeta T}, \tag{71}$$

where

$$\pi = \pi^{00} - \pi^{zz}. \tag{72}$$

It is easy to show that the above formulas reduce to the ones in the first-order theory if one takes $\tau_\pi \to 0$ and $\tau_\Pi \to 0$. We remark here that, contrary to the first-order theory, one needs to specify initial conditions for dissipative currents in the second-order theory.

3.6 Summary

Let us summarize the main points so far as follows:

- hydrodynamics is a framework to describe the space–time evolution of matter under local thermal equilibrium;
- a naïve extension of the Navier–Stokes equation to its relativistic version, which is called the first-order theory, has problems on instabilities and causality;
- relaxation terms are needed in the constitutive equations to resolve the above issues;
- these terms naturally arise in the constitutive equations when the second-order corrections of dissipative currents are considered in the entropy current.

4 Applications

In this section we apply the formalism of hydrodynamics to heavy-ion collisions. As already noted in Sect. 1, we do not argue recent analyses in terms of viscous hydrodynamics. We show only results from ideal hydrodynamic models. One can also consult recent other reviews of hydrodynamic models at RHIC which complement the present lecture note [46–53]. We start by discussing some basic tests of whether the system produced in H.I.C. can be described by thermodynamic quantities. Then we discuss collective flow and introduce ideal hydrodynamic models to describe the flow phenomena in H.I.C. Finally we show results from ideal hydrodynamic models and compare them with experimental data.

4.1 Basic Checks of Observables at RHIC

Recent lattice QCD results show [54] that the energy density as a function of the temperature suddenly increases by ~ 1 GeV/fm^3 at the (pseudo-)critical temperature $T_c \sim 190$ MeV.[10] Above this temperature, the system is supposed to be in the deconfined QGP. The first check is whether the energy density produced in H.I.C. is sufficient to form a QGP. Phenomenologically, the energy density in H.I.C. can be estimated through Bjorken's formula [16][11]

$$\epsilon_{\mathrm{Bj}}(\tau) = \frac{\langle m_T \rangle}{\tau \pi R^2} \frac{dN}{dy} . \tag{73}$$

Here $\langle m_T \rangle$ is the mean transverse mass, $y = \frac{1}{2} \ln \frac{E+p_z}{E-p_z}$ is the rapidity, $\frac{dN}{dy}$ is the number of particles per unit rapidity, $\tau = \sqrt{t^2 - z^2}$ is the proper time, and R is an effective transverse radius. The energy density obtained above depends on the proper time since the system is supposed to expand in the longitudinal direction with the expansion scalar $\theta = 1/\tau$. One can compare Bjorken's energy density to the energy density from lattice QCD simulations to see whether it is sufficient energy density to form a QGP. Figure 3 shows the PHENIX data on $\varepsilon_{\mathrm{Bj}}\tau$ versus the number of participants at three collision energies [57, 58]. If τ is taken to be 1 fm/c, Bjorken's energy densities at $\sqrt{s_{NN}} = 130$ and 200 GeV are well above the energy density at the transition region ~ 1 GeV/fm^3. Therefore, sufficient energy is deposited in the central rapidity region in H.I.C. at RHIC. However, attention

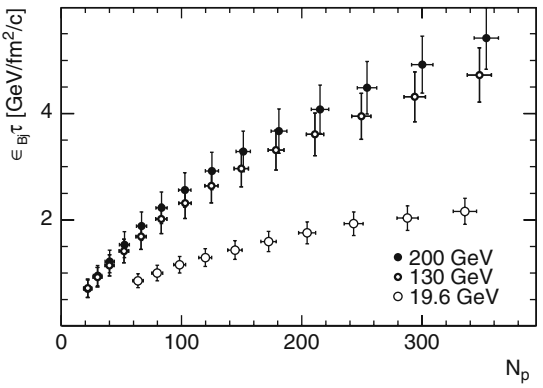

Fig. 3 $\varepsilon_{\mathrm{Bj}}\tau$ versus the number of participants at three collision energies [57, 58]

[10] Energy density increases with temperature rapidly but smoothly. So this is not a phase transition but a crossover in a thermodynamically strict sense. This is the reason why we call it pseudo-critical temperature here.

[11] This formula neglects the effect of pdV work. If the system is kinetically equilibrated, the energy density should be larger than the value obtained by this formula [55, 56].

should be paid to the interpretation. The above formula just counts the total measured energy divided by the volume of a cylinder. So the system is not necessarily thermalized. In this sense, this is a necessary condition, not a sufficient condition, to form a QGP.

The next basic check is whether the matter in H.I.C. reaches chemical equilibrium. Assuming thermal and chemical equilibria, we can calculate the number density of a certain particle species

$$n_i(T,\mu) = \frac{g}{2\pi^2}\int_0^\infty \frac{p^2 dp}{\exp\left[(E_i-\mu_i)/T\right]\pm 1}\,. \tag{74}$$

n_i gives the number density of particle species i as a function of the temperature T and chemical potential μ_i. g is the degeneracy of the particle, p is the momentum, and E is the energy. We further assume that the measured particle number is fixed at a certain temperature and chemical potential, which is called chemical freezeout. Then the average number of particles, $\langle N_i\rangle$, can be estimated by summing contribution from particles directly emitted from the system with volume V and contribution from resonance decays

$$\langle N_i\rangle = V\left[n_i^{\rm th}(T,\mu) + \sum_R \Gamma_{R\to i} n_R(T,\mu)\right]. \tag{75}$$

Here $n_i^{\rm th}$ and n_R are the number density of directly emitted particle i and resonance R, respectively. $\Gamma_{R\to i}$ is the branching ratio of the resonance R decaying into species i. When one looks at ratios of two particle numbers, the volume V is canceled out. Thus the particle ratios depend only on two parameters: the temperature T and the baryonic chemical potential μ_B. In Fig. 4, various combinations of the particle ratio observed at RHIC are fitted by two parameters [59]. We find a remarkably good fit

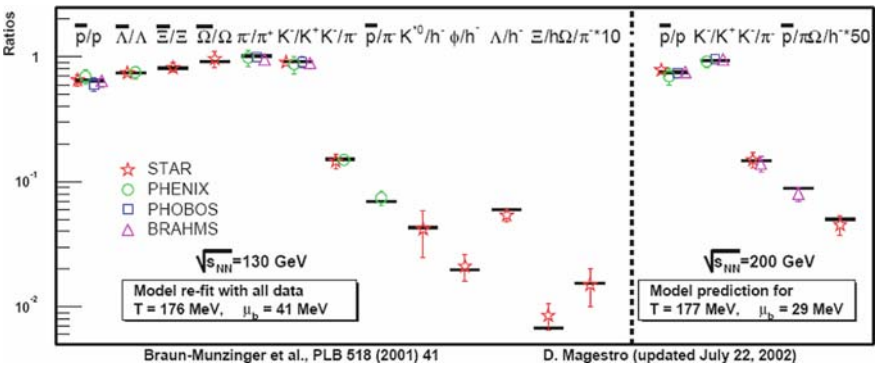

Fig. 4 Ratios of particle numbers produced at RHIC [59]

to data with only these two parameters.[12] At $\sqrt{s_{NN}} = 130$ GeV, the temperature is fitted to be 176 MeV which is close to the critical temperature from lattice QCD calculations. At the temperature, which we call chemical freezeout temperature T^{ch}, the system ceases to be in chemical equilibrium. So we expect that the system reaches chemical equilibrium above T^{ch}. Again, one has to keep in mind that this is a necessary condition since even in e^+e^- or pp collisions observed particle ratios are fitted reasonably well by using statistical models [60, 61]. See also discussions in, e.g., [62, 63]. The last basic check is whether the matter reaches kinetic equilibrium. If we suppose a system in H.I.C. is in kinetic equilibrium, the pressure is built inside the system. The matter is surrounded by vacuum, so pressure gradient in outward directions generates collective flow and, in turn, the system expands radially. The momentum distribution in kinetically equilibrated matter is isotropic. On the other hand, when the matter is moving at a finite velocity the momentum distribution is Lorentz boosted. This is illustrated in Fig. 5. If this kind of distortion in momentum distribution can be observed experimentally, one can obtain some information about kinetic equilibrium. Assuming each fluid element expands radially at radial flow velocity v_T, the p_T spectra for pions and protons can be calculated by convoluting these distorted momentum distributions over azimuthal direction (blast wave model [64, 65]). Here p_T is the transverse momentum which is perpendicular to the collision axis. The green curves are results with $T = 100$ MeV and radial flow velocity $v_T = 0.5$. On the other hand, the red curves are results with $T = 160$ MeV and vanishing flow $v_T = 0$. For light particles like pions, there is almost no sensitivity to

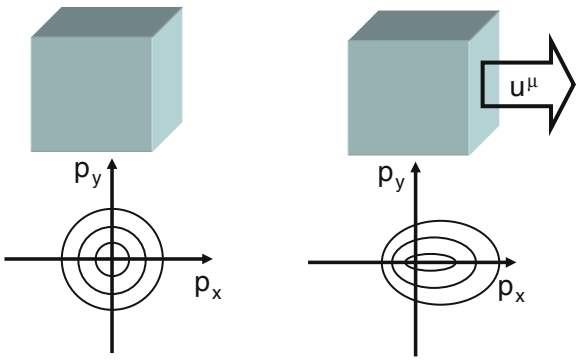

(a) Isotropic case (b) Lorentz boosted in positive x direction

Fig. 5 Fluid elements at rest and at a finite velocity in x-direction. Momentum distribution in the latter case is distorted by Lorentz boost along x-axis

[12] There are some additional parameters in the recent statistical models such as excluded volume correction, strangeness suppression factor, and so on for a better description of the data.

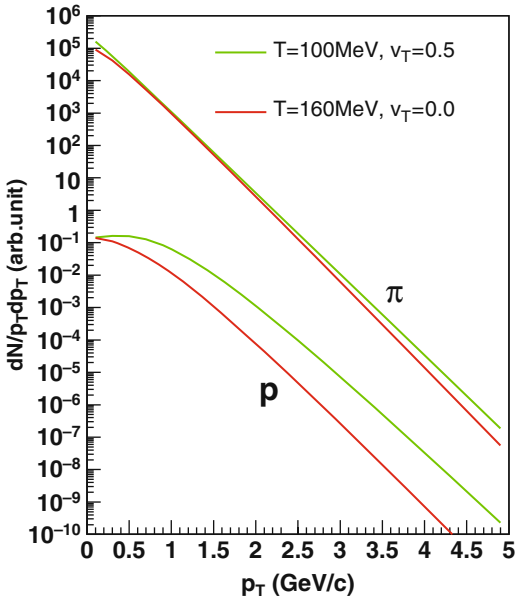

Fig. 6 p_T spectra for pions and protons from a thermal plus boost picture. See text for details

distinguish the two cases: Reduction of temperature is almost compensated by radial flow. However, in the case of heavier particles like protons, a clear difference can be seen between these two cases: There is a shoulder structure at low p_T resulting from radial flow. This kind of spectral change is observed in H.I.C., as can be seen in Fig. 7. It shows the proton p_T spectra for p+p (black), d+Au (pink), and Au+Au (red) collisions obtained by STAR Collaboration [66]. For p+p and d+Au collisions the spectra have just a power law shape. However, in Au+Au collisions, one sees a shoulder structure at low p_T (< 1 GeV/c). This is consistent with a thermal plus boost picture and suggests that a large pressure could be built up in Au+Au collisions. One can fit the p_T spectrum using a blast wave parametrization [64, 65] and obtains decoupling temperature $T^{\rm dec}$ and the mean collective flow velocity as a function of the centrality. Even for pp collisions these parameters are finite (see Fig. 8) [67], which indicates that a more sophisticated model would be needed to interpret the data. This kind of spectral change can also be seen in results from kinetic theories in which kinetic equilibrium is not fully achieved. Therefore it is indispensable to perform a systematic study based on a more sophisticated dynamical framework.

We have obtained the necessary conditions for studying the QGP: (1) The energy density can be well above the critical value which is predicted from lattice QCD simulations; (2) A chemical freezeout temperature extracted from particle ratios is close to pseudo-critical temperature which is again from lattice QCD simulations; (3) High pressure can be built up in H.I.C., which suggests the system reaches

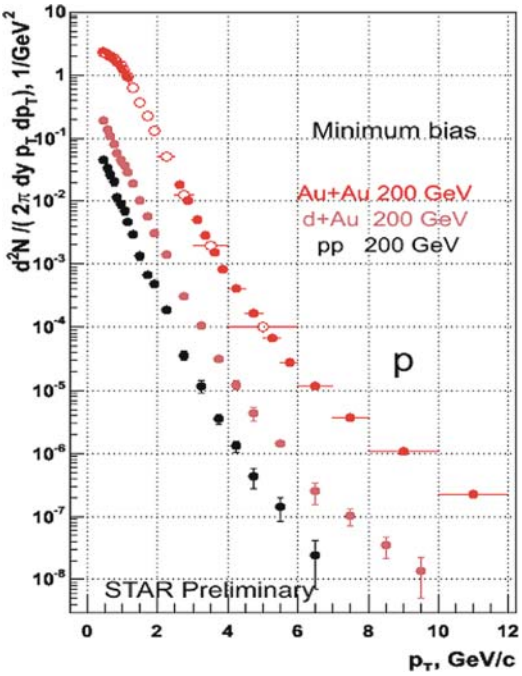

Fig. 7 Proton spectrum for pp (*black*), dAu (*pink*), and Au+Au (*red*) collisions. Adopted from a presentation file by O. Barannikova at Quark Matter 2005, Budapest, Hungary [66]

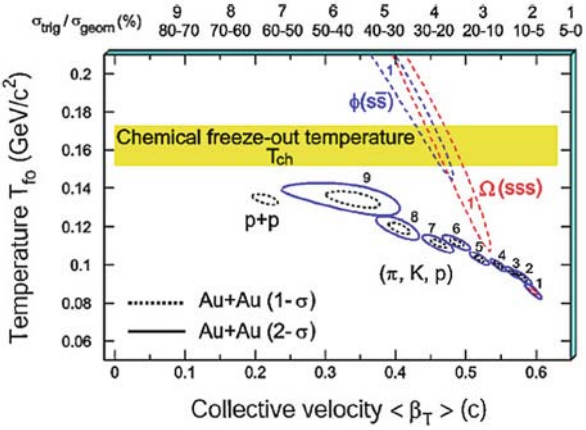

Fig. 8 Fitted parameters in blast wave model calculations [67]

kinetic equilibrium. If one of them was not confirmed through these basic checks, one would not need to go to the next steps toward detailed studies of the QGP in H.I.C.

4.2 Elliptic Flow

Before going to a detailed discussion on the hydrodynamic models, we discuss collective flow, in particular, anisotropic transverse flow. Here "collective flow" is meant by the correlation between position of matter and direction of flow, which is not necessary to be hydrodynamically evolving matter. A good example has already appeared in the previous subsection. In the case of radial flow, velocity of expanding matter has a component parallel to the radial coordinate. Figure 9 shows a heavy-ion collision in the reaction plane (left) and transverse plane (right). In such a collision a region of the locally equilibrated state can be created. In the transverse plane the overlap region has an almond-like shape, so the region is anisotropic with respect to the azimuthal angle. The azimuthal momentum distribution can be expanded into a Fourier series[13]

$$\frac{dN}{d\phi} = \frac{N}{2\pi}\left[1 + 2v_1\cos(\phi) + 2v_2\cos(2\phi) + \cdots\right], \tag{76}$$

$$v_n = \frac{\int d\phi \cos(n\phi)\frac{dN}{d\phi}}{\int d\phi \frac{dN}{d\phi}} = \langle\cos(n\phi)\rangle, \tag{77}$$

where ϕ is the azimuthal angle of momentum and v_n are the Fourier coefficients of nth harmonics [68]. Because of the symmetry around the y-axis the sine terms vanish. The first and second harmonics, v_1 and v_2, are called directed and elliptic flow parameters, respectively. The first harmonic, v_1, is illustrated in Fig. 10a. Particles are emitted preferably, e.g., in the direction of the large arrows in the reaction plane.

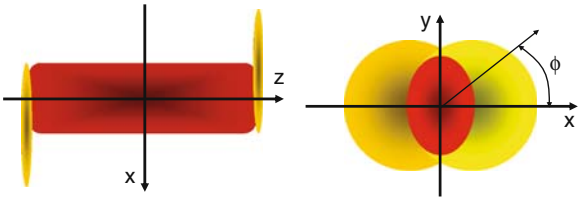

(a) In the reaction plane (b) In the transverse plane

Fig. 9 Illustration of a H.I.C.

[13] Here we suppose azimuthal angle is measured from reaction plane. Of course, in the experimental situations, the reaction plane is not known a priori. We will not go into details of how to find reaction plane experimentally.

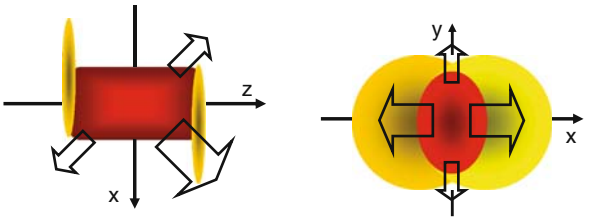

(a) First harmonic v_1 (b) Second harmonic v_2

Fig. 10 Anisotropic transverse flow

Directed flow is significantly seen near the beam rapidity region but vanishes near midrapidity due to symmetry of the collision geometry. The second harmonic, v_2, is much more relevant for studying matter around midrapidity in H.I.C. at relativistic energies since spectators already fly away [69], therefore a lot of efforts to measure v_2 have been made at RHIC so far. One of the first observables was actually v_2 measured by STAR Collaboration [70]. It is illustrated in Fig. 10b.

Elliptic flow is how the system responds to the initial spatial anisotropy [69, 71–73]. Suppose two extreme situations illustrated in Fig. 11. In the first case (see Fig. 11a) the mean free path among the produced particles is much larger than the typical size of the system. In this case the azimuthal distribution of particles does not depend on azimuthal angle on average due to the symmetry of the production process. The other extreme case is when the mean free path is very small compared to the typical system size (see Fig. 11b). In this case hydrodynamics can be applied to describe the space–time evolution of the system. The pressure gradient along the horizontal axis is much larger than that along the vertical axis due to the geometry.

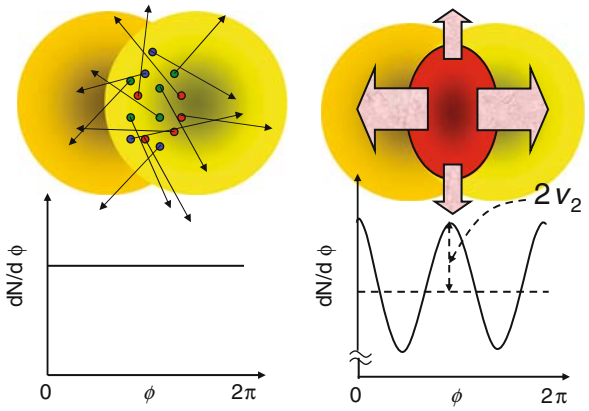

(a) Large mean free path (b) Small mean free path

Fig. 11 Normalized azimuthal distribution $dN/d\phi$ of a noncentral H.I.C.

So the collective flow is enhanced along the horizontal axis rather than along the vertical axis and, in turn, the azimuthal distribution gets oscillated. The amplitude of this oscillation in the normalized azimuthal distribution describes exactly the elliptic flow parameter. In this way, the elliptic flow is generated by the spatial anisotropy of the almond shape due to multiple interactions among the produced particles. We have good opportunities to extract some information about the mean free path from the elliptic flow analysis.

The eccentricity is a very important quantity to interpret elliptic flow phenomena. To quantify the initial almond shape, the following formula can be used:

$$\varepsilon = \frac{\langle y^2 - x^2 \rangle}{\langle y^2 + x^2 \rangle} . \tag{78}$$

The brackets denote an average over the transverse plane with the number density of participants as a weighting function

$$\langle \cdots \rangle = \int dx dy \cdots n_{\text{part}}(x, y) . \tag{79}$$

This is sometimes called the standard eccentricity. If the system is elongated along the y-axis, the eccentricity is positive. In more realistic situations, the eccentricity fluctuates from event to event. This fluctuation of the initial eccentricity [74–79] is important to understand the elliptic flow in the small system such as Cu+Cu collisions or peripheral Au+Au collisions. Figure 12 shows a sample event projected into the transverse plane from a Monte Carlo Glauber model. Participants are shown in magenta and spectators are in yellow and orange. In this case one could misidentify the tilted line as the reaction plane, while the true reaction plane is the horizontal axis (dashed line). The angle of the tilted plane with respect to the true reaction plane fluctuates event by event. Of course we cannot observe the true reaction plane from experimental data. On the other hand, an apparent reaction

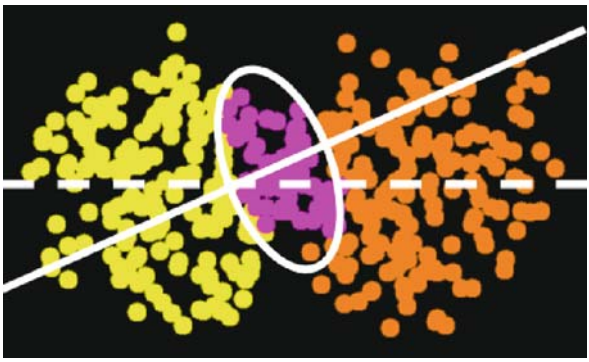

Fig. 12 An example of participants (*magenta*) and spectators (*yellow* and *orange*) in a H.I.C. from a Monte Carlo Glauber model. Adopted from a presentation file by D. Hofman at Quark Matter 2006, Shanghai, China

plane (tilted line in Fig. 12) is determined also by elliptic flow signal itself. Another definition, called the participant eccentricity, is much more relevant for quantifying the almond shape in the event-by-event basis

$$\varepsilon_{\text{part}} = \frac{\sqrt{(\sigma_y^2 - \sigma_x^2)^2 + 4\sigma_{xy}^2}}{\sigma_x^2 + \sigma_y^2}\,, \tag{80}$$

$$\sigma_x^2 = \left\{x^2\right\} - \{x\}^2\,, \tag{81}$$

$$\sigma_y^2 = \left\{y^2\right\} - \{y\}^2\,, \tag{82}$$

$$\sigma_{xy} = \{xy\} - \{x\}\{y\}\,. \tag{83}$$

Now the average $\{\cdots\}$ is taken over in a single event generated by a Monte Carlo Glauber model.

In the following, the important properties of elliptic flow are demonstrated through hydrodynamic/transport simulations of H.I.C. In hydrodynamic simulations, the eccentricity is usually defined by weighting local energy density $e(x, y)$ or local entropy density $s(x, y)$ in the transverse plane rather than the number density of participants $n_{\text{part}}(x, y)$. Figure 13 shows the eccentricity ε_x and the momentum eccentricity

$$\varepsilon_p = \frac{\int dxdy(T_0^{xx} - T_0^{yy})}{\int dxdy(T_0^{xx} + T_0^{yy})} \tag{84}$$

as a function of the proper time from a hydrodynamic simulation assuming Bjorken scaling solution in the longitudinal direction and two different sets of the EoS [46]. Details of hydrodynamic models will be discussed later. The spatial eccentricity ε_x decreases as the system expands and the momentum anisotropy rapidly increases at the same time. So the spatial anisotropy turns into the momentum anisotropy. The momentum anisotropy ε_p is created and saturates in the first several femtometers, so the observed v_2 is expected to be sensitive to the initial stage of the collision. Figure 14 shows the impact parameter dependence of the ratio of output (v_2) to input

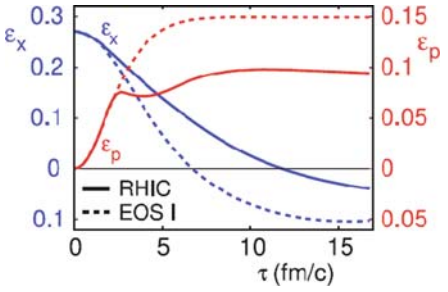

Fig. 13 The spatial eccentricity ε_x and the momentum eccentricity ε_p as a function of the proper time τ in Au+Au collisions at $b = 7$ fm [46]. *Solid* and *dashed curves* correspond to two different sets of the EoS

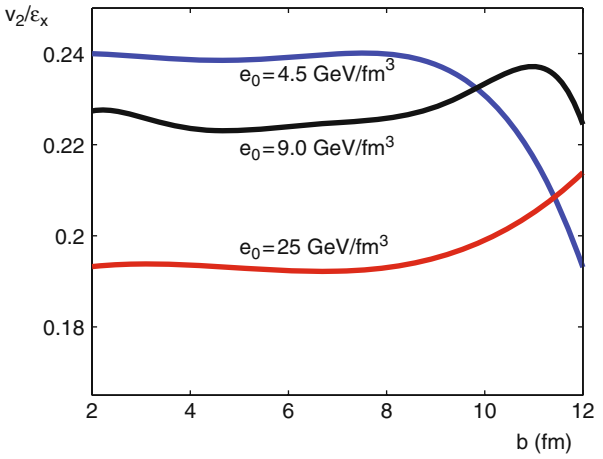

Fig. 14 v_2/ε_x as a function of impact parameter b [80]

(ε_x) [80] which can be understood as a response of the system. Ideal hydrodynamics predicts that v_2 is roughly proportional to the eccentricity

$$v_2 \approx 0.2\varepsilon\,. \tag{85}$$

Figure 15 shows a result from a kinetic approach based on the Boltzmann equation for gluons undergoing elastic scattering only [81].[14] Starting with a uniform distribution in an almond shape in coordinate space and thermal distribution in

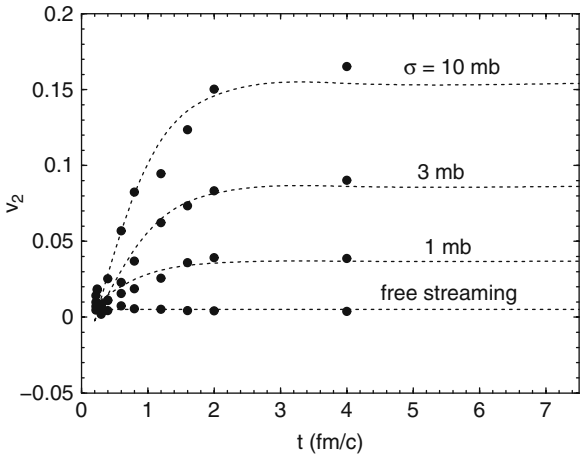

Fig. 15 v_2 as a function of proper time from Boltzmann calculations for different gluon cross sections [81]. *Curves* are guide to eyes

[14] Inelastic scattering ($gg \leftrightarrow ggg$) is implemented in a kinetic approach only recently. Although this is a higher-order process in perturbative expansion, it turns out to affect elliptic flow significantly. See [82–84]

momentum space, the multi-gluon system expands according to the Boltzmann equation with various transport cross sections.[15] From this figure we can understand several important features of the elliptic flow:

1. v_2 is not generated in the free-streaming case, so elliptic flow is generated indeed through secondary collisions;
2. elliptic flow is generated in the early stage of the collision and saturates after the first 2 to 3 fm/c;
3. the saturated value of v_2 is sensitive to the cross section among the particles

$$\sigma_{\rm tr} \propto \frac{1}{\lambda} \propto \frac{1}{\eta}\,, \tag{86}$$

   where λ is the mean free path and η is the shear viscosity calculated in the kinetic theory of gases;
4. in the limit of large transport cross sections (strongly interacting limit), the system is expected to reach the ideal hydrodynamic result[16] since $\eta \to 0$.

Through measurement of v_2 and its analysis in terms of hydrodynamic/transport models, one can extract the transport properties of the matter produced in H.I.C. In the next subsection, we discuss hydrodynamic modeling of H.I.C.

4.3 Ideal Hydrodynamic Model

Hydrodynamics introduced in Sect. 3 is a general framework to describe the space–time evolution of locally thermalized matter for a given equation of state (EoS). This framework has been applied to the intermediate stage in H.I.C. In this section, we neglect the effects of dissipation and concentrate on discussion about ideal hydrodynamic models. The main ingredient in ideal hydrodynamic models in H.I.C. is the EoS of hot and dense matter governed by QCD. In addition, one also needs to assign initial conditions to the hydrodynamic equations. Hydrodynamics can be applied to a system in which local thermalization is maintained. However, in the final state of H.I.C. the particles are freely streaming toward the detectors and their mean free path is almost infinite. This is obviously beyond the applicability of hydrodynamics. Hence we also need a description to decouple the particles from the rest of the system. To summarize, the hydrodynamic modeling of H.I.C. needs an EoS, initial conditions, and a decoupling prescription. Modeling of these ingredients in hydrodynamic simulations has been sophisticated for these years and tested against a vast body of RHIC data.

---

[15] In kinetic theories, momentum exchanges among particles are responsible for equilibration. However, forward scattering with very small scattering angle is insufficient for the system to equilibrate. So the effective (transport) cross section can be defined as $\sigma_{\rm tr} = \int d\theta_{\rm cm} \sin^2\theta_{\rm cm} \frac{d\sigma}{d\theta_{\rm cm}}$, where $\theta_{\rm cm}$ is scattering angle in the center of mass system between two scattering particles.

[16] The Boltzmann equation is applied to *dilute* gases where two-particle correlation can be ignored. So one should keep in mind the applicability condition of the kinetic theory in this case.

We first look at the EoS in more detail. The EoS is in principle calculated from lattice QCD simulations. The realistic results with (almost) physical quark masses are obtained recently [54]. However, if one wants to utilize the EoS from lattice simulations, one needs to interpret the EoS in terms of a hadron picture [85] since one calculates momentum distributions of hadrons in the final decoupling stage. For this purpose, the lattice EoS is compared with the resonance gas model below T_c. If there exists a deviation between them, it prevents one from utilizing the lattice EoS directly in hydrodynamic simulations. Instead, in hydrodynamic simulations, the models of EoS depicted in Fig. 16 are conventionally used [46]. The most simple EoS (EOS I) is $P = e/3$ for an ideal gas of relativistic massless particles.[17] A more realistic EoS (EOS Q) includes the effect of hadron masses and phase transition between hadronic matter and the QGP. At low energy density the EoS is described by a hadron resonance gas model (EOS H). This particular model includes almost all the hadrons in the Particle Data Table [86], while some models include only ground states of hadron multiplets or several low mass resonances. At high energy density, the EoS can be described by a bag model

$$P = \frac{1}{3}(e - 4B)\,. \tag{87}$$

The bag constant B is tuned to match pressure of the QGP phase to that of a hadron resonance gas at critical temperature T_c: $P_{\mathrm{QGP}}(T_c) = P_{\mathrm{hadron}}(T_c)$. As discussed in Sect. 4.1, a hadron gas in H.I.C. is not in chemical equilibrium below the chemical freezeout temperature. T^{ch} is closed to T_c, so the hadron phase may not be chemically equilibrated in H.I.C. A chemically frozen hadron resonance gas can be described by introducing the chemical potential for each hadron [87–93]. The numbers $\tilde{N}_i$ including all decay contributions from higher-lying resonances, $\tilde{N}_i = N_i + \sum_R b_{R\to iX} N_R$, are conserved during the evolution in co-moving frame

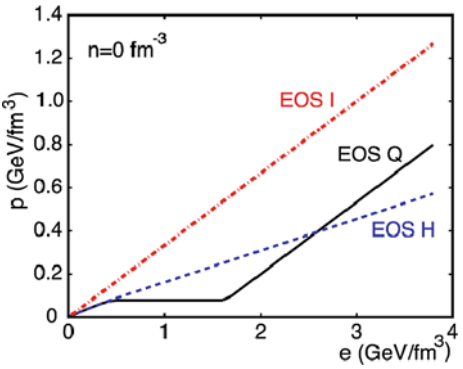

Fig. 16 Some typical EoS in hydrodynamic models [46]

[17] This EoS is always obtained in relativistic conformal field theories in which the trace of energy–momentum tensor is vanishing $T^{\mu}{}_{\mu} = e - 3P = 0$. So the particles are not necessarily "free."

of fluid elements. Here N_i is the number of the ith hadronic species in a fluid element and $b_{R\to iX}$ is the effective branching ratio (a product of branching ratio and degeneracy) of a decay process $R \to i+X$. One can calculate the chemical potential as a function of temperature from the following conditions:

$$\frac{\tilde{n}_i(T,\mu_i)}{s(T,\{\mu_i\})} = \frac{\tilde{n}_i(T_c,\mu_i=0)}{s(T_c,\{\mu_i\}=0)}\,. \tag{88}$$

Instead of solving continuity equations for each hadron, the effect of hadron number conservation can be embedded in the EoS of resonance gas through $\mu_i(T)$ obtained above. For a decoupling prescription, the Cooper–Frye formula [94] is almost a unique choice to convert the hydrodynamic picture to the particle picture

$$E\frac{dN}{d^3p} = \int_\Sigma f(x,p,t)p\cdot d\sigma(x) \tag{89}$$

$$= \frac{d}{(2\pi)^3}\int_\Sigma \frac{p\cdot d\sigma(x)}{\exp\left[(p\cdot u(x)-\mu(x))/T(x)\right]\pm 1}\,, \tag{90}$$

where E is the energy, f is the phase space distribution, d the degeneracy of the particle under consideration (e.g., $d=3$ for pions), p is the momentum, $d\sigma$ is the normal vector to the freezeout surface element, u is the four-velocity, μ is the chemical potential, and T is the decoupling temperature assuming isothermal freezeout hypersurface Σ. Contribution from resonance decays should be taken into account by applying some decay kinematics to the outcome of the Cooper–Frye formula. The decoupling temperature $T^{\rm dec}$ is fixed through *simultaneous* fitting of p_T spectra for various hadrons in the low p_T region. In the blast wave model, decoupling temperature and radial flow velocity are independent parameters to fit p_T spectra. On the other hand, there is a negative correlation between $T^{\rm dec}$ and average radial flow velocity in the hydrodynamic model: the lower decoupling temperature, the larger average radial flow velocity. This formula ensures the energy–momentum conservation on freezeout hypersurface Σ as long as the EoS is calculated using the same distribution function. If one puts resonances up to the mass of 2 GeV in the resonance gas model, one should calculate all the contribution of hadrons in the EoS. Otherwise, neglect of the contribution leads to violation of the energy momentum conservation.[18] It should be noted that $p\cdot d\sigma$ term in Eq. (90) can be negative. This means the incoming particles through Σ are counted as a negative number. Although this seems peculiar, this negative contribution is needed for global energy–momentum conservation.

The prescription to calculate the momentum distribution as above is sometimes called the sudden freezeout model since the mean free path of the particles changes from zero (ideal fluid) to infinity (free streaming) within a thin layer Σ. Although this model is too simple, it has been used in hydrodynamic calculations for a long

[18] If the lattice EoS below T_c cannot be described by a resonance gas model, the Cooper–Frye formula violates the energy–momentum conservation on Σ. This is the reason why there are only few serious attempts of lattice EoS to hydrodynamic simulations.

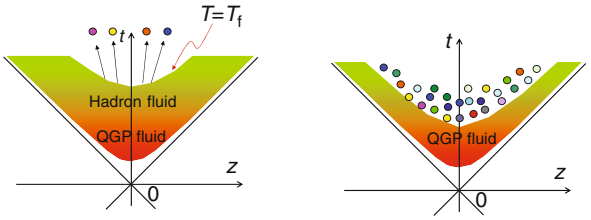

(a) Sudden freezeout (b) Gradual freezeout

Fig. 17 Two freezeout pictures in H.I.C.

time. It is illustrated in Fig. 17a. Recently one utilizes hadronic cascade models to describe the gradual freezeout [95–99]. As will be shown, this hadronic afterburner is mandatory in understanding v_2 data. Phase space distributions for hadrons are initialized below T_c by using the Cooper–Frye formula. The hadronic cascade models describe the space–time evolution of the hadron gas. This model is illustrated in Fig. 17b. This kind of hybrid approaches in which the QGP fluids are followed by hadronic cascade models automatically describes both the chemical and the thermal freezeout and is much more realistic especially for the late stage.

Initial conditions in hydrodynamic simulations are so chosen as to reproduce the centrality and rapidity dependences of multiplicity $dN_{\rm ch}/d\eta$. Initial conditions here mean energy density distribution $e(x, y, \eta_s)$ and flow velocity $u^\mu(x, y, \eta_s)$ at the initial time τ_0. Again baryon density is neglected since, at midrapidity at RHIC, the net baryon density is quite small. The pressure distribution can be obtained from the energy density distribution through the EoS. Space–time rapidity η_s, independent initial energy density distribution $e(x, y, \eta_s) = e(x, y)$, and Bjorken scaling solution $u^\mu_{\rm Bj}$ are assumed in $(2+1)$-dimensional hydrodynamic simulations. In this case, one discuss as the observables only at midrapidity. At $\eta_s = 0$, one can parametrize [100] the initial entropy density based on the Glauber model

$$s(x, y) = \frac{dS}{\tau_0 d\eta_s d^2x_\perp} \propto \alpha n_{\rm part}(x, y; b) + (1-\alpha) n_{\rm coll}(x, y; b). \tag{91}$$

The soft/hard fraction α is adjusted to reproduce the measured centrality dependence [101] of the charged hadron multiplicity at midrapidity. By using the EoS, one can calculate the initial energy density distribution from Eq. (91). For fully three-dimensional initial conditions, see [87, 97, 102]. A novel initial condition is based on the color glass condensate (CGC) picture [103]. One can calculate the local energy density of produced gluons within the CGC framework [104–106] and utilize it as an initial condition of hydrodynamic simulations. In Fig. 18, an example of the CGC initial energy density distribution for a noncentral H.I.C. in a full $(3 + 1)$-dimensional hydrodynamic simulation [107] is shown in the transverse plane (left) and in the reaction plane (right). In the right side panel the horizontal axis corresponds to the impact parameter direction and the vertical axis to the

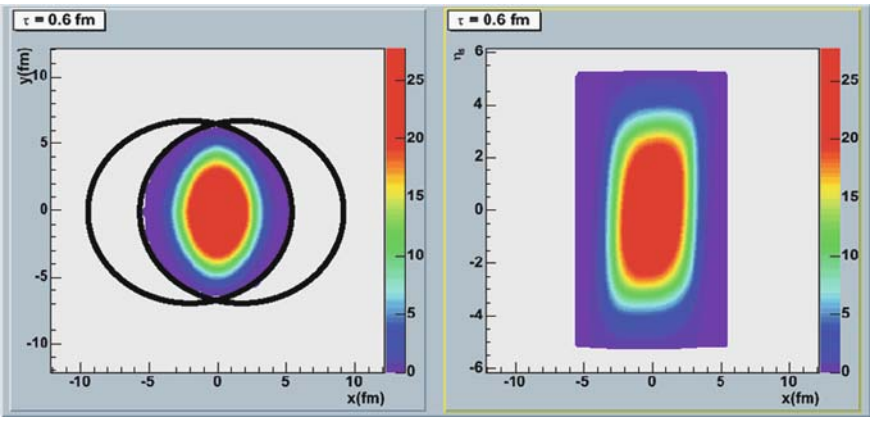

Fig. 18 Energy density distribution in a noncentral H.I.C. within a CGC initial condition in the transverse plane (*left panel*) and in the reaction plane (*right panel*). The two horizontal *thick black lines* in the right panel are the Lorentz contracted nuclei. The color gradation in the right side of each panel indicates the energy density scale in unit of GeV/fm^3

space–time rapidity η_s. Figures 19 and 20 show charged particle multiplicity from hydrodynamic simulations that are compared with the PHOBOS data [101, 108]. Figure 19 shows $dN_{\rm ch}/d\eta$ as a function of the number of participants ($N_{\rm part}$) [101]. These data are fitted by using two kinds of initial conditions: from Glauber model calculations and from color glass condensate (CGC) model calculations [97]. Both models reproduce the centrality dependence of the data. Figure 20 shows the rapidity distribution of $dN_{\rm ch}/d\eta$ for each centrality [108]. The fitting of multiplicity is the starting point of further analysis based on hydrodynamic simulations.

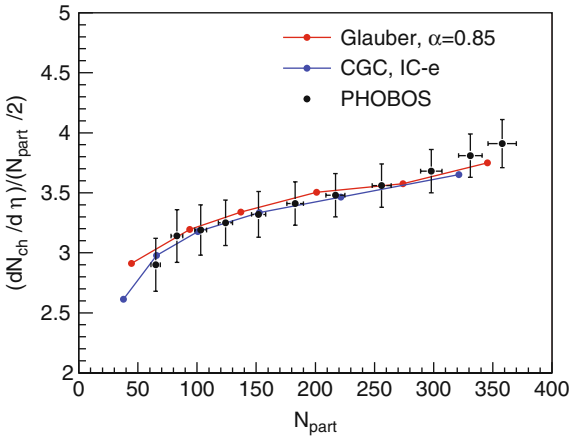

Fig. 19 Centrality dependence of multiplicity from PHOBOS [108] are fitted by hydrodynamic calculations with two different initial conditions [97, 107]

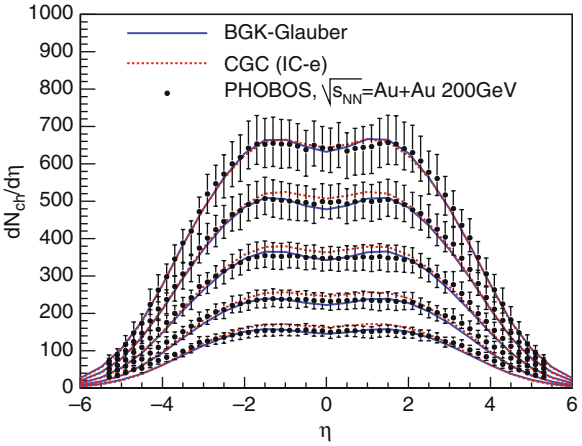

Fig. 20 Pseudorapidity dependence of multiplicity from PHOBOS [108] is fitted by hydrodynamic calculations with two different initial conditions [97, 107]

In the hydrodynamic models, various combinations of initial conditions, EoS and decoupling prescriptions, are available to analyze the experimental data in H.I.C. Of course, final results largely depend on modeling of each ingredient. So it is quite important to constrain each model and its inherent parameters through systematic analyses of the data toward a comprehensive understanding of the QGP.

4.4 Application of the Ideal Hydrodynamic Model to H.I.C.

In this subsection we analyze H.I.C. at RHIC in terms of ideal hydrodynamic models discussed in the previous subsection.

Before we start our main discussion on elliptic flow parameter v_2, we mention here that the transverse momentum distributions for pions, kaons, and protons are also important since these reflect dominant transverse flow, namely radial flow. Currently, among hydrodynamic models, yields and slopes of p_T spectra are reproduced in pure hydrodynamic calculations with early chemical freezeout or in gradual freezeout approaches. It should be noted here that simultaneous reproduction of the yields and the slopes is important. Sometimes, one only compares the slope of the p_T spectra by scaling the yields "by hand" within hydrodynamic approaches. However, chemical composition of hadronic matter does affect the transverse expansion [87]. Therefore, it does not make any sense if one compares only the slopes by keeping chemical equilibrium of hadrons.

As discussed in Sect. 4.2, v_2/ε can be interpreted as a response of the system to initial spatial eccentricity. Figure 21 shows v_2/ε as a function of the transverse multiplicity density $(1/S)dN_{\rm ch}/dy$ from AGS to RHIC energies. Hydrodynamic results in Fig. 14 are shown symbolically as horizontal lines. The experimental data monotonically increase with particle density, while ideal hydrodynamic response is

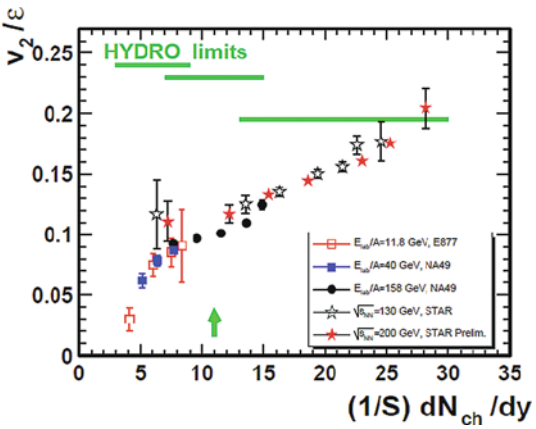

Fig. 21 v_2/ε as a function of transverse multiplicity density compiled by NA49 Collaboration [109]

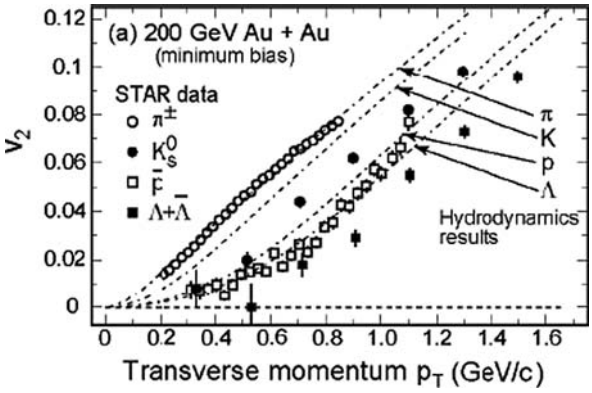

Fig. 22 Differential v_2 for pions, kaons, protons, and lambdas [67]

almost flat [80]. Ideal hydrodynamics is expected to generate the maximum response among the transport models.[19] The experimental data reach this limit for the first time at RHIC. Figure 22 shows the differential elliptic flow v_2 as a function of transverse momentum for pions, kaons, protons, and lambdas. A mass ordering pattern is seen in v_2 data, which was predicted by ideal hydrodynamic calculations [110].[20] The pseudorapidity dependence of v_2 observed by PHOBOS [111] has a triangular

[19] It should be emphasized again that the hydrodynamic results above are obtained by a particular combination of modeling, i.e., Glauber-type initial conditions, EOS Q with chemical equilibrium in the hadron phase and sudden freezeout at fixed decoupling temperature.

[20] There is a caveat to interpret the agreement since this particular hydrodynamic calculation does not reproduce particle ratios due to a lack of early chemical freezeout. The importance of hadronic viscosity and chemical freezeout in hydrodynamic calculations is recognized [112] after the announcement of the discovery of perfect fluid QGP [2].

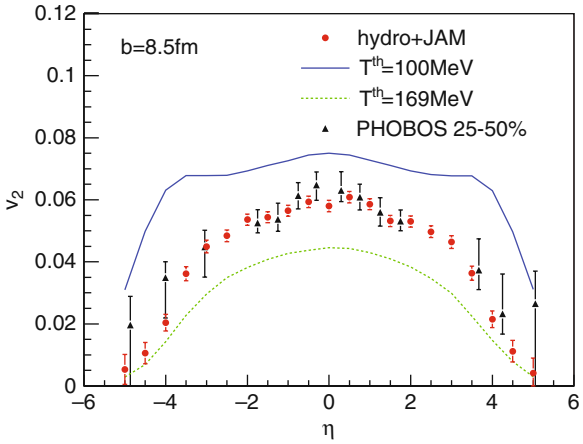

Fig. 23 Pseudorapidity dependence of v_2. PHOBOS data [111] compared to different model calculations [97]

shape as is seen in Fig. 23. In the pure ideal hydrodynamic result, hydrodynamic equations are initialized by the Glauber model and are solved all the way down to $T^{\rm dec} = 100\,{\rm MeV}$. The pure hydrodynamic model gives a comparable result with the data only at midrapidity. However, at forward and backward rapidities, it overshoots the data significantly. If we replace the hadron fluid with a hadron gas utilizing a hadron cascade, v_2 is significantly reduced in the forward and backward regions. In this hybrid model the hadrons have a finite mean free path, which results in an effective shear viscosity in the hadron phase. So dissipative hadronic "corona" effects turn out to be important in understanding the v_2 data. The model also reproduces a mass ordering pattern of v_2 for identified hadrons as a function of p_T near

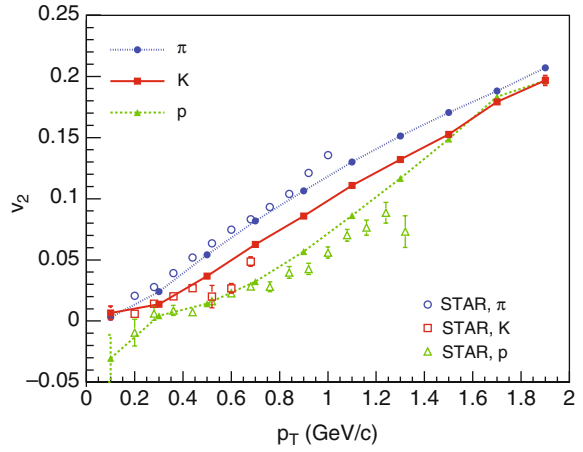

Fig. 24 Differential v_2. STAR data [67] compared to model calculations [98]

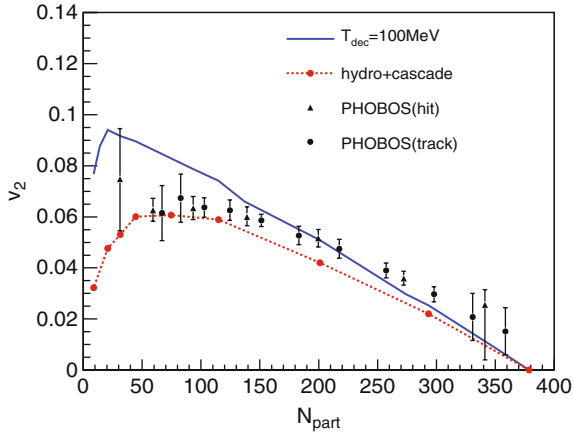

Fig. 25 v_2 as a function of centrality. PHOBOS data [111] compared to different model calculations [97]

midrapidity in Fig. 24. Figure 25 shows the centrality dependence of v_2. The solid line is the result from ideal hydrodynamic calculations while the dotted line is from the hybrid model. It is clear that for peripheral collisions, where the multiplicity is small, the hadronic viscosity plays an important role. One may notice that the result from the hybrid model is systematically and slightly smaller than the data. However, there could exist the effect of initial eccentricity fluctuations which is absent in this hydrodynamic calculations. The deviation between the results and the data can be interpreted quantitatively by this effect. Figure 26 shows $v_2(p_T)$ for pions, kaons,

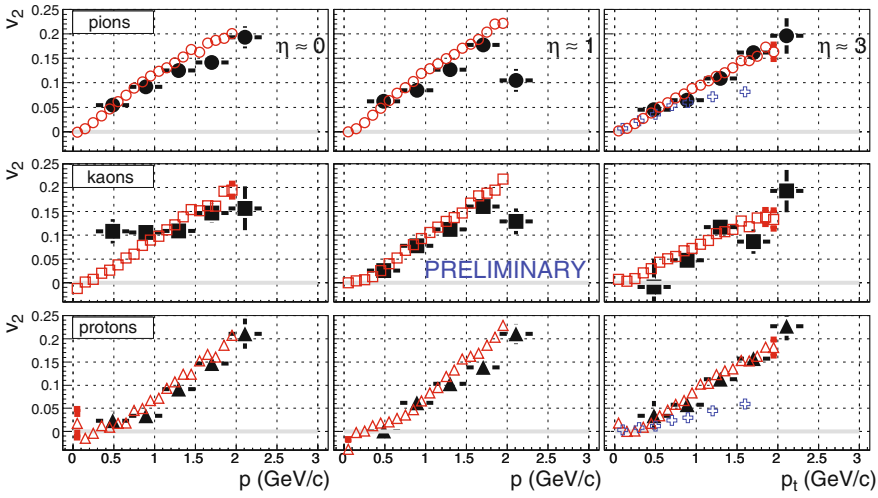

Fig. 26 Differential v_2 for pions, kaons, and protons for $\eta = 0$ (*left*), $\eta = 1$ (*middle*), and $\eta = 3$ (*right*) [113]

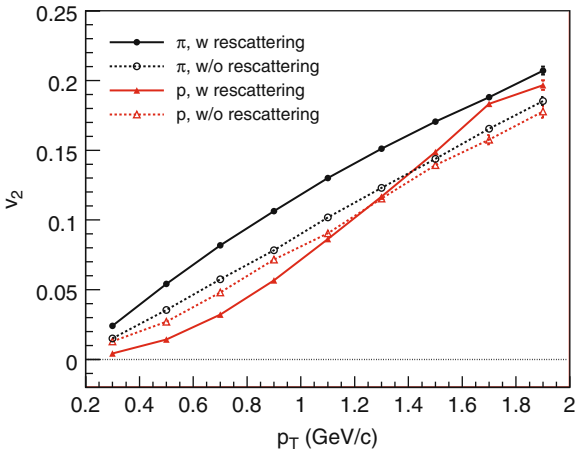

Fig. 27 Differential v_2 with and without hadronic rescattering [98]

and protons in 10–50% centrality at $\eta = 0$ (left), $\eta = 1$ (middle), and $\eta = 3$ (right) observed by BRAHMS [113]. Also here the hybrid model reproduces the p_T slope of these differential elliptic flow parameters.

We would like to point out here that the mass ordering, clearly visible in Fig. 24, is there in the final result. If one would look at the result just after the QGP phase transition, the difference between the pions and the protons would be quite small. So it turns out that the splitting patterns are caused by hadronic rescattering. This is illustrated in Fig. 27. One can conclude that the large magnitude of the integrated v_2 and the strong mass ordering of the differential $v_2(p_T)$ observed at RHIC result from a subtle interplay between perfect fluid dynamics of the early QGP stage and dissipative dynamics of the late hadronic stage: The large magnitude of v_2 is due to the large overall momentum anisotropy, generated predominantly in the early QGP stage, whereas the strong mass splitting behavior at low p_T reflects the redistribution of this momentum anisotropy among the different hadron species, driven by the continuing radial acceleration and cooling of the matter during the hadronic rescattering phase.

We have seen so far that the hydrodynamic model which includes Glauber-type initial conditions followed by a perfect fluid QGP and a dissipative hadronic gas evolution is the most successful combination for describing the RHIC data. We now go to the discussion on the initialization dependence of v_2. Two types of initial conditions, namely the Glauber-type initial conditions and the CGC initial conditions, are discussed in the previous subsection. v_2 as a function of centrality is shown again for these two initial conditions in Fig. 28. In the case of the Glauber initial conditions we can conclude early thermalization and the discovery for the perfect fluid QGP. In the case of the CGC initial conditions, we cannot, however, claim the discovery since the model initialized by CGC overshoots the data in almost the whole range. Since the hydrodynamic model calculations depend on the initial con-

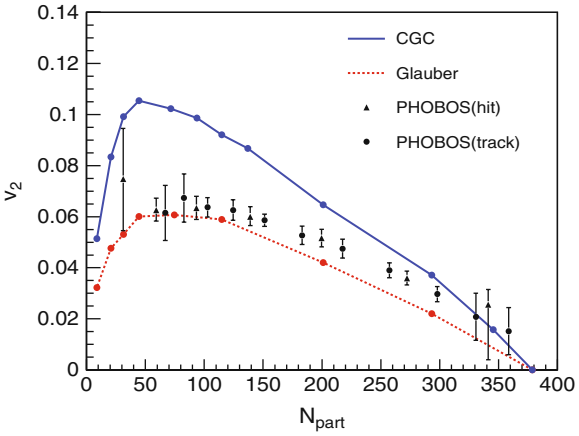

Fig. 28 v_2 as a function of centrality. PHOBOS data [111] are compared to hydrodynamic results with two different sets of initial conditions [97]

ditions, it is very important to understand them before making final conclusions. In the case of CGC initial conditions viscosity might be needed even in the QGP phase to get the model down to the data points. The effect of viscosity could therefore be quite important. The high v_2 values from the CGC initial conditions are traced back to the initial eccentricity. In Fig. 29a the energy density distribution in the impact parameter direction is plotted for different conditions. If the energy density profile has a sharp edge (no diffuseness), an integral in Eq. (78) is relatively weighted in the edge region and, consequently, eccentricity becomes maximum at a given impact parameter. If one compares the energy density profile of the CGC with the one of the Glauber model, one sees that the CGC profile has a sharper edge than the Glauber model does. The resultant eccentricity as a function of impact parameter is shown in Fig. 29b. Eccentricity from the CGC is about 20–30% larger than that from the

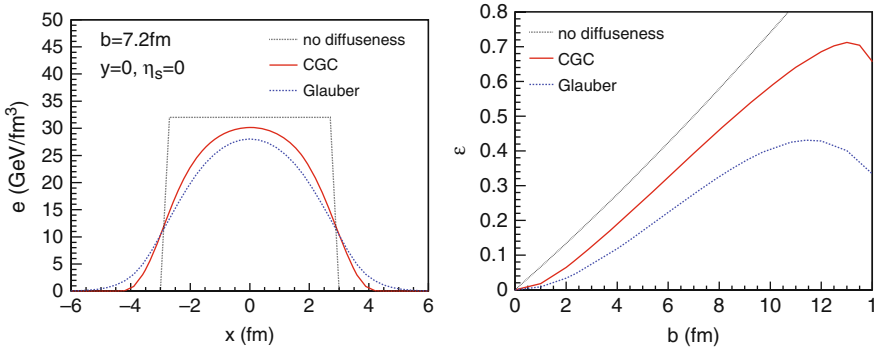

(a) Energy density distribution (b) Initial eccentricity

Fig. 29 The difference eccentricity between Glauber and CGC initial conditions

Glauber model. This is the reason why hydro + hadronic cascade approach which even includes hadronic viscosity overshoots the v_2 data.[21]

4.5 Summary

Hydrodynamics is a framework to describe the space–time evolution of matter under local equilibrium. It is applied to the intermediate stage in H.I.C. to extract the transport properties of the QGP from RHIC data. Hydrodynamic modeling includes initial conditions, EoS, and decoupling prescriptions. Final results certainly depend on combination of each modeling. So much attention should be paid to these ingredients before drawing robust conclusions from hydrodynamic analyses. Elliptic flow has played a major role in understanding the transport properties of the QGP. Glauber initial conditions, ideal hydrodynamics in the QGP phase, and dissipative gas for the hadron phase are three pillars for agreement between the model and the elliptic flow data. Whereas, if CGC initial conditions are employed, the initial eccentricity gets increased by 20–30%. If the nature chooses this kind of initial condition, viscosity might be needed even in the QGP phase.

Acknowledgments One of the authors (T.H.) is much indebted to M. Gyulassy, T. Hatsuda, U. Heinz, T. Kunihiro, S. Muroya, M. Natsuume, and Y. Nara for fruitful discussion. The work of T.H. was partly supported by Grant-in-Aid for Scientific Research No. 19740130. One of the authors (A.B.) would like to thank Despoina Evangelakou for technical support during the writing of the lecture note.

References

1. http://www.veccal.ernet.in/qm2008.html 139
2. http://www.bnl.gov/bnlweb/pubaf/pr/PR_display.asp ?prID=05–38 140, 171
3. M. Gyulassy, I. Vitev, X.N. Wang and B.W. Zhang: arXiv:nucl-th/0302077 141
4. A. Kovner and U.A. Wiedemann: arXiv:hep-ph/0304151 141
5. T. Matsui and H. Satz: Phys. Lett. **B 178**, 416 (1986) 141
6. T. Peitzmann and M.H. Thoma: Phys. Rept. **364**, 175 (2002) 141
7. D.G. d'Enterria and D. Peressounko: Eur. Phys. J. **C 46**, 451 (2006) 141
8. C. Eckart: Phys. Rev. **58**, 919 (1940) 142, 145
9. C. Cattaneo: Atti. Sem. Mat. Fis. Univ. Modena **3**, 83 (1948) 153
10. L.D. Landau, E.M. Lifshitz: *Fluid Mechanics*, pp. 133–136, Pergamon Press, New York (1959) 145
11. M. Namiki and C. Iso: Prog. Theor. Phys. **18**, 591 (1957)
12. C. Iso, K. Mori and M. Namiki: Prog. Theor. Phys. **22**, 403 (1959)
13. I. Müller: Z. Phys. **198**, 329 (1967)
14. W. Israel: Ann. Phys. **100**, 310 (1976)
15. W. Israel and J.M. Stewart: Ann. Phys. **118**, 341 (1979)
16. J.D. Bjorken: Phys. Rev. **D 27**, 140 (1983) 150, 151, 155

[21] See also recent more realistic calculations of eccentricity within a CGC framework [76].

17. A. Hosoya and K. Kajantie: Nucl. Phys. **B 250**, 666 (1985)
18. P. Danielewicz and M. Gyulassy: Phys. Rev. **D 31**, 53 (1985)
19. L.P. Csernai: *Introduction to Relativistic Heavy Ion Collisions*, John Wiley & Sons, New York (1994)
20. J.P. Blaizot and J.Y. Ollitrault: Adv. Ser. Direct. High Energy Phys. **6**, 393 (1990)
21. R. Maartens: arXiv:astro-ph/9609119 147
22. D.H. Rischke: arXiv:nucl-th/9809044
23. I. Müller: Living Rev. Rel. **2**, 1 (1999)
24. J.Y. Ollitrault: Eur. J. Phys. **29**, 275 (2008) 142
25. P. Kovtun, D.T. Son and A.O. Starinets: Phys. Rev. Lett. **94**, 111601 (2005) 151
26. A. Nakamura and S. Sakai: Phys. Rev. Lett. **94**, 072305 (2005) 151
27. D. Kharzeev and K. Tuchin: arXiv:0705.4280 [hep-ph] 152
28. F. Karsch, D. Kharzeev and K. Tuchin: Phys. Lett. **B 663**, 217 (2008) 152
29. M. Mizutani, S. Muroya and M. Namiki: Phys. Rev. **D 37**, 3033 (1988) 152
30. W.A. Hiscock and L. Lindblom: Phys. Rev. **D 31**, 725 (1985) 152
31. G.S. Denicol, T. Kodama, T. Koide and Ph. Mota: arXiv:0807.3120 [hep-ph] 152
32. A. Muronga: Phys. Rev. Lett. **88**, 062302 (2002) 153
33. A. Muronga: Phys. Rev. Lett. **89**, 159901 (2002) [Erratum]
34. A. Muronga: Phys. Rev. **C 69**, 034903 (2004)
35. A. Muronga: Phys. Rev. **C 76**, 014909 (2007)
36. A. Muronga: Phys. Rev. **C 76**, 014910 (2007)
37. U.W. Heinz, H. Song and A.K. Chaudhuri: Phys. Rev. **C 73**, 034904 (2006)
38. H. Song and U.W. Heinz: Phys. Lett. **B 658**, 279 (2008)
39. R. Baier, P. Romatschke and U.A. Wiedemann: Phys. Rev. **C 73**, 064903 (2006)
40. R. Baier, P. Romatschke and U.A. Wiedemann: Nucl. Phys. **A 782**, 313 (2007)
41. R. Baier and P. Romatschke: Eur. Phys. J. **C 51**, 677 (2007)
42. P. Romatschke: Eur. Phys. J. **C 52**, 203 (2007)
43. P. Romatschke and U. Romatschke: Phys. Rev. Lett. **99**, 172301 (2007)
44. K. Dusling and D. Teaney: Phys. Rev. **C 77**, 034905 (2008)
45. T. Koide, G.S. Denicol, Ph. Mota and T. Kodama: Phys. Rev. **C 75**, 034909 (2007) 153
46. P.F. Kolb and U.W. Heinz: arXiv:nucl-th/0305084 154, 163, 166
47. P. Huovinen: arXiv:nucl-th/0305064
48. P. Huovinen and P.V. Ruuskanen: Ann. Rev. Nucl. Part. Sci. **56**, 163 (2006)
49. T. Hirano: Acta Phys. Pol. **B 36**, 187 (2005)
50. T. Hirano: Prog. Theor. Phys. Suppl. **168**, 347 (2007)
51. Y. Hama, T. Kodama and O. Socolowski Jr.: Braz. J. Phys. **35**, 24 (2005)
52. F. Grassi: Braz. J. Phys. **35**, 52 (2005)
53. C. Nonaka: J. Phys. **G 34**, S313 (2007) 154
54. M. Cheng et al.: Phys. Rev. **D 77**, 014511 (2008) 155, 166
55. M. Gyulassy and T. Matsui: Phys. Rev. **D 29**, 419 (1984) 155
56. P.V. Ruuskanen: Phys. Lett. **B 147**, 465 (1984) 155
57. S.S. Adler et al. [PHENIX Collaboration]: Phys. Rev. **C 71**, 034908 (2005) 155
58. S.S. Adler et al. [PHENIX Collaboration]: Phys. Rev. **C 71**, 049901 (2005) [Erratum] 155
59. P. Braun-Munzinger, K. Redlich and J. Stachel: arXiv:nucl-th/0304013 156
60. F. Becattini and U.W. Heinz: Z. Phys. **C 76**, 269 (1997) 157
61. F. Becattini and U.W. Heinz: Z. Phys. **C 76**, 578 (1997) [Erratum] 157
62. D.H. Rischke: Nucl. Phys. **A 698**, 153 (2002) 157
63. V. Koch: Nucl. Phys. **A 715**, 108 (2003) 157
64. P.J. Siemens and J.O. Rasmussen: Phys. Rev. Lett. **42**, 880 (1979) 157, 158
65. E. Schnedermann, J. Sollfrank and U.W. Heinz: Phys. Rev. **C 48**, 2462 (1993) 157, 158
66. O. Barannikova [STAR Collaboration]: Nucl. Phys. **A 774**, 465 (2006) 158, 159
67. J. Adams et al. [STAR Collaboration]: Nucl. Phys. **A 757**, 102 (2005) 158, 159, 171, 172
68. A.M. Poskanzer and S.A. Voloshin: Phys. Rev. **C 58**, 1671 (1998) 160

69. J.Y. Ollitrault: Phys. Rev. **D 46**, 229 (1992) 161
70. K.H. Ackermann et al. [STAR Collaboration]: Phys. Rev. Lett. **86**, 402 (2001) 161
71. H. Heiselberg and A.M. Levy: Phys. Rev. **C 59**, 2716 (1999) 161
72. H. Sorge: Phys. Rev. Lett. **82**, 2048 (1999)
73. S.A. Voloshin and A.M. Poskanzer: Phys. Lett. **B 474**, 27 (2000) 161
74. M. Miller and R. Snellings: arXiv:nucl-ex/0312008 162
75. X.I. Zhu, M. Bleicher and H. Stoecker: Phys. Rev. **C 72**, 064911 (2005)
76. H.J. Drescher and Y. Nara: Phys. Rev. **C 75**, 034905 (2007) 176
77. R. Andrade, F. Grassi, Y. Hama, T. Kodama and O. Socolowski Jr.: Phys. Rev. Lett. **97**, 202302 (2006)
78. W. Broniowski, P. Bozek and M. Rybczynski: Phys. Rev. **C 76**, 054905 (2007)
79. B. Alver et al.: Phys. Rev. **C 77**, 014906 (2008) 162
80. P.F. Kolb, J. Sollfrank and U.W. Heinz: Phys. Rev. **C 62**, 054909 (2000) 164, 171
81. B. Zhang, M. Gyulassy and C.M. Ko: Phys. Lett. **B 455**, 45 (1999) 164
82. Z. Xu and C. Greiner: Phys. Rev. **C 71**, 064901 (2005) 164
83. Z. Xu and C. Greiner: Phys. Rev. **C 76**, 024911 (2007)
84. Z. Xu and C. Greiner: Phys. Rev. Lett. **100**, 172301 (2008) 164
85. F. Karsch, K. Redlich and A. Tawfik: Eur. Phys. J. **C 29**, 549 (2003) 166
86. C. Amsler et al.: Phys. Lett. **B 667**, 1 (2008) 166
87. T. Hirano and K. Tsuda: Phys. Rev. **C 6**6, 054905 (2002) 166, 168, 170
88. H. Bebie, P. Gerber, J.L. Goity and H. Leutwyler: Nucl. Phys. **B 378**, 95 (1992)
89. N. Arbex, F. Grassi, Y. Hama and O. Socolowski Jr.: Phys. Rev. **C 64**, 064906 (2001)
90. W.L. Qian, R. Andrade, F. Grassi, Y. Hama and T. Kodama: arXiv:0709.0845 [nucl-th]
91. D. Teaney: nucl-th/0204023
92. P.F. Kolb and R. Rapp: Phys. Rev. **C 67**, 044903 (2003)
93. P. Huovinen: arXiv:0710.4379 [nucl-th] 166
94. F. Cooper and G. Frye: Phys. Rev. **D 10**, 186 (1974) 167
95. S.A. Bass and A. Dumitru: Phys. Rev. **C 61**, 064909 (2000) 168
96. D. Teaney, J. Lauret and E.V. Shuryak: Phys. Rev. Lett. **86**, 4783 (2001)
97. T. Hirano, U.W. Heinz, D. Kharzeev, R. Lacey and Y. Nara: Phys. Lett. **B 636**, 299 (2006) 168, 169, 170, 172, 173, 175
98. T. Hirano, U.W. Heinz, D. Kharzeev, R. Lacey and Y. Nara: Phys. Rev. **C 77**, 044909 (2008) 172, 174
99. C. Nonaka and S.A. Bass: Phys. Rev. **C 75**, 014902 (2007) 168
100. T. Hirano: Phys. Rev. **C 65**, 011901 (2002) 168
101. P.F. Kolb, U.W. Heinz, P. Huovinen, K.J. Eskola and K. Tuominen: Nucl. Phys. **A 696**, 197 (2001) 168, 169
102. B.B. Back et al. [PHOBOS Collaboration]: Phys. Rev. **C 65**, 061901 (2002) 168
103. E. Iancu and R. Venugopalan: arXiv:hep-ph/0303204 168
104. D. Kharzeev and E. Levin: Phys. Lett. **B 523**, 79 (2001) 168
105. D. Kharzeev, E. Levin and M. Nardi: Nucl. Phys. **A 730**, 448 (2004)
106. D. Kharzeev, E. Levin and M. Nardi: Nucl. Phys. **A 743**, 329 (2004) [Erratum] 168
107. T. Hirano and Y. Nara: Nucl. Phys. **A 743**, 305 (2004) 168, 169, 170
108. B.B. Back et al.: Phys. Rev. Lett. **91**, 052303 (2003) 169, 170
109. C. Alt et al. [NA49 Collaboration]: Phys. Rev. **C 68**, 034903 (2003) 171
110. P. Huovinen, P.F. Kolb, U.W. Heinz, P.V. Ruuskanen and S.A. Voloshin: Phys. Lett. **B 503**, 58 (2001) 171
111. B.B. Back et al. [PHOBOS Collaboration]: Phys. Rev. **C 72**, 051901 (2005) 171, 172, 173, 175
112. T. Hirano and M. Gyulassy: Nucl. Phys. **A 769**, 71 (2006) 171
113. S.J. Sanders: J. Phys. **G 34**, S1083 (2007) 173, 174